Brain Structure and Function (2021) 226:1067–1098
https://doi.org/10.1007/s00429-021-02226-7

ORIGINAL ARTICLE

Investigating the effects of healthy cognitive aging on brain functional connectivity using 4.7 T resting-state functional magnetic resonance imaging

Stanislau Hrybouski[1] · Ivor Cribben[1,2] · John McGonigle[3] · Fraser Olsen[4] · Rawle Carter[5] · Peter Seres[4] · Christopher R. Madan[6] · Nikolai V. Malykhin[1,4,5]

Received: 7 July 2020 / Accepted: 20 January 2021 / Published online: 18 February 2021

Abstract

Functional changes in the aging human brain have been previously reported using functional magnetic resonance imaging (fMRI). Earlier resting-state fMRI studies revealed an age-associated weakening of intra-system functional connectivity (FC) and age-associated strengthening of inter-system FC. However, the majority of such FC studies did not investigate the relationship between age and network amplitude, without which correlation-based measures of FC can be challenging to interpret. Consequently, the main aim of this study was to investigate how three primary measures of resting-state fMRI signal—network amplitude, network topography, and inter-network FC—are affected by healthy cognitive aging. We acquired resting-state fMRI data on a 4.7 T scanner for 105 healthy participants representing the entire adult lifespan (18–85 years of age). To study age differences in network structure, we combined ICA-based network decomposition with sparse graphical models. Older adults displayed lower blood-oxygen-level-dependent (BOLD) signal amplitude in all functional systems, with sensorimotor networks showing the largest age differences. Our age comparisons of network topography and inter-network FC demonstrated a substantial amount of age invariance in the brain's functional architecture. Despite architecture similarities, old adults displayed a loss of communication efficiency in our inter-network FC comparisons, driven primarily by the FC reduction in frontal and parietal association cortices. Together, our results provide a comprehensive overview of age effects on fMRI-based FC.

Keywords High-field fMRI · Resting-state fMRI · Brain aging · Network amplitude · Sparse graphs

Introduction

Many cognitive functions decline with age (Buckner 2004; Grady 2008, 2012; Fabiani 2012; Hedden and Gabrieli 2004; Reuter-Lorenz and Cappell 2008; Schneider-Garces et al. 2010; Spreng et al. 2010). Although the cognitive neuroscience literature tends to emphasize aging effects on high-level cognition, especially memory, task switching, and selective attention (Fabiani 2012; Li et al. 2015; Spreng et al. 2010), laboratory tests of visual perception, facial processing, and motor function also revealed a drop in performance with age (Grady et al. 1994; Houx and Jolles 1993; Kauranen and Vanharanta 1996; Mattay et al. 2002). It has been hypothesized that brain physiology alterations are responsible for much of the age-related decline in cognitive capacity (Buckner 2004; Grady 2008, 2012; Reuter-Lorenz and Cappell 2008; Sperling 2007; Spreng et al. 2010).

✉ Nikolai V. Malykhin
nikolai@ualberta.ca

1 Neuroscience and Mental Health Institute, University of Alberta, Edmonton, AB, Canada

2 Department of Accounting and Business Analytics, Alberta School of Business, University of Alberta, Edmonton, AB, Canada

3 Department of Brain Sciences, Imperial College London, London, UK

4 Department of Biomedical Engineering, University of Alberta, Edmonton, AB, Canada

5 Department of Psychiatry, Faculty of Medicine and Dentistry, University of Alberta, Edmonton, AB T6G 2V2, Canada

6 School of Psychology, University of Nottingham, Nottingham, UK

The human brain can be conceptualized as a highly structured network, sometimes termed as the connectome of dynamically interacting neuronal communities (Buckner et al. 2013; Power et al. 2011; Rubinov and Sporns 2010; Wig 2017; Yeo et al. 2011, 2014). The brain's functional architecture is commonly estimated from spontaneous low-frequency blood-oxygen-level-dependent (BOLD) signal fluctuations, measured during resting-state functional Magnetic Resonance Imaging (RS-fMRI) scans (Buckner et al. 2013; Craddock et al. 2013; Smith et al. 2011; Wig 2017; Wig et al. 2014). Functional connectivity (FC) studies report 7–20 major resting-state networks (RSNs) with network topography localized to visual, somatomotor, and cognitive regions of the brain (Allen et al. 2011; Christoff et al. 2016; Gordon et al. 2017; Laumann et al. 2015; Petersen and Posner 2012; Power et al. 2011; Raichle and Snyder 2007; Wig 2017; Yeo et al. 2011). Since spatial profiles of many RSNs resemble activation patterns from task-based fMRI studies, it has been hypothesized that RSNs represent fundamental units of brain organization, which are recruited in various combinations to perform specific tasks (Buckner et al. 2013; Crossley et al. 2013; Deco and Corbetta 2011; Smith et al. 2009; Spreng et al. 2010).

Much of the early work on the relationship between resting-state FC and age was focused on intra-network communication in select RSNs, especially the default mode system (e.g., Andrews-Hanna et al. 2007; Damoiseaux et al. 2008; Grady et al. 2012; Hampson et al. 2012; Koch et al. 2010; Onoda et al. 2012; Persson et al. 2014; Sambataro et al. 2010). Those studies revealed an age-related loss of functional interaction between the medial frontal and the posterior cingulate/retrosplenial cortices (but see Persson et al. 2014). More recent RS-fMRI studies showed that in addition to the default mode network (DMN), age-related reduction in within-system FC is also present in brain networks involved in attention, cognitive control, sensory processing, and motor function (Allen et al. 2011; Betzel et al. 2014; Grady et al. 2016; Ng et al. 2016; Song et al. 2014; Spreng et al. 2016; Zonneveld et al. 2019). Moreover, studies that employed graphical models to quantify age effects on FC showed that network community structure becomes less efficient and less segregated in old age (Cao et al. 2014; Chan et al. 2014; Chong et al. 2019; Geerligs et al. 2015; Spreng et al. 2016), with long-range FC being particularly vulnerable (Tomasi and Volkow 2012).

Despite these advances, the number of studies that examined age differences in functional architecture of the entire brain is still relatively small, with most relying on anatomical or functional atlases to define their networks (Betzel et al. 2014; Chan et al. 2014; Chong et al. 2019; Fjell et al. 2015; Geerligs et al. 2015; Meunier et al. 2009; Song et al. 2014; Wang et al. 2010). Unfortunately, it has been shown that FC estimates can vary substantially from one atlas to another, even when all image preprocessing and data analysis methods are controlled (Cao et al. 2014). Employing ROIs from a predefined atlas may also fail to capture inter-individual variability in brain organization since individual network architecture can deviate, sometimes substantially, from an average map (Gordon et al. 2017; Laumann et al. 2015; Mueller et al. 2013). Furthermore, most connectomic studies of brain aging used mass univariate correlation methods to quantify age effects on the brain's functional organization (Andrews-Hanna et al. 2007; Betzel et al. 2014; Geerligs et al. 2015; Grady et al. 2016; Han et al. 2018; Meier et al. 2012; Rubinov and Sporns 2010; Zonneveld et al. 2019). Although informative, correlation-based differences are challenging to interpret without additional information about the underlying BOLD signal properties (Duff et al. 2018). In addition to the time series coupling, two other factors are responsible for the correlation coefficient strength in all RS-fMRI connectivity comparisons: network amplitude and magnitude of background noise (Duff et al. 2018). For this reason, examining network amplitude adds another layer of valuable information about the underlying neurobiology of aging. It also provides insight into factors that may have caused the observed increases/decreases in correlation-based FC. To date, research on the relationship between age and RSN amplitude has been limited. Most RS-fMRI studies of brain aging did not test for age differences in network amplitude (e.g., Betzel et al. 2014; Cao et al. 2014; Chan et al. 2014; Geerligs et al. 2015; Grady et al. 2016; Meunier et al. 2009; Spreng et al. 2016), while those that did, focused either on early (up to middle adulthood) or late (50 years of age and older) aging only (Allen et al. 2011; Zonneveld et al. 2019).

Since conclusions from many prior RS-fMRI studies of brain aging were limited by correlation-only methodology, our study's main goal was to investigate age effects on every primary measure of RS-fMRI signal—i.e., network amplitude, network topography, and inter-network communication. To address these research questions, we combined a high-field RS-fMRI acquisition, data-driven network decomposition, sparse graphical model estimation, and a sample representing the entire adult lifespan. In task-based fMRI experiments, the most prominent activity differences between young and old adults are often found in the prefrontal and parietal association cortices (Cabeza et al. 2002, 2004; Davis et al. 2008; Grady et al. 1994; Gutchess et al. 2005; Li et al. 2015; Logan et al. 2002; Persson et al. 2014; Rypma and D'Esposito 2000; Rajah and D'Esposito 2005; Schneider-Garces et al. 2010; Spreng et al. 2010; Sugiura, 2016). Consequently, we were also interested in determining whether RSNs mapping onto frontal and parietal association areas are more affected by aging than visual, auditory, and somatomotor RSNs.

Since previous task-based and resting-state fMRI studies reported aging-related reductions of BOLD signal power in a variety of cortical areas (Allen et al. 2011; D'Esposito et al. 1999; Handwerker et al. 2007; Hesselmann et al. 2001; Mehagnoul-Schipper et al. 2002; Riecker et al. 2006; Taoka et al. 1998; West et al. 2019; Zonneveld et al. 2019), we predicted a widespread decline of BOLD signal amplitude with age affecting multiple RSNs. According to recent boundary-based FC work (Han et al. 2018), network structure does not change drastically with age. Consequently, we expected a large degree of architectural stability throughout the adult lifespan. Lastly, since previous structural and functional imaging work showed frontal and parietal association cortices to be particularly vulnerable to aging processes (Grady et al. 2016; Damoiseaux 2017; Fabiani 2012; Raz et al. 2005; Sugiura 2016; Wig 2017), we expected frontal and parietal association networks to display the largest age differences in FC and BOLD signal amplitude.

Materials and methods

Participants

For this cross-sectional study, we recruited 105 healthy volunteers (45 men, 60 women) across the entire adult lifespan (16 volunteers per decade of life, on average; age range: 18–85; Table 1) through online, newspaper, and poster advertisements. Of those, 78 participants were Caucasian (74%), 17 Asian (16%), 7 Latin American (7%), 2 (2%) Persian and 1 Arab (1%) Canadians. According to the 20-item Edinburgh Handedness Inventory (Oldfield 1971), 12 of the participants were left-handed [individuals with laterality quotient $\geq +80$ were determined as right-handed]. All participants had no lifetime psychiatric disorders and no reported psychosis or mood disorders in first-degree relatives, as assessed by the Anxiety Disorders Interview Schedule—IV (Brown et al. 2001; Di Nardo et al. 1994), which assesses for anxiety, affective, and substance use disorders. Medical exclusion criteria were defined as those active and inactive medical conditions that may interfere with normal cognitive function: cerebrovascular pathology, all tumors or congenital malformations of the nervous system, diabetes, multiple sclerosis, Parkinson's disease, epilepsy, organic psychosis (other than dementia), schizophrenia, and stroke. Furthermore, medications that directly affect cognition, including benzodiazepines, antipsychotics, anticholinergic drugs, and antidepressants, were also exclusionary. The participants' demographic information is summarized in Table 1.

In-person interviews were conducted to assess each participant's cognitive function. Older subjects with mild cognitive impairment (MCI) and dementia were excluded from the study. MCI was defined by the presence of cognitive complaints (documented on the AD-8, Galvin et al. 2007) with documented impairment on the Montreal Cognitive Assessment (MOCA) test (Nasreddine et al. 2005). All of our participants attained MOCA scores between 26 and 30. Dementia was defined according to the DSM-IV criteria with Clinical Dementia Rating (CDR) as an additional screening tool in older (> 50 years of age) participants (Hughes et al. 1982). CDR was used to assess functional performance in

Table 1 Age-specific demographic information of study participants

	Age group		
	Young ($n=43$)	Middle ($n=31$)	Old ($n=31$)
Age (years)			
Mean ± SD	27.1 ± 5.4	50.0 ± 5.6	70.3 ± 6.7
Range [min/max]	18/39	41/59	61/85
Sex (males/females)	18/25	13/18	14/17
Handedness (left/right)	5/38	5/26	2/29
Smoking history (y/n)	2/41	1/30	1/30
Elevated blood pressure (y/n)	0/43	1/30	12/19
Family history of AD (y/n)	7/36	4/27	6/25
Education (years)			
Mean ± SD	16.2 ± 1.8	16.0 ± 2.5	15.7 ± 3.0
Range [min/max]	12/20	12/22	11/23
MOCA			
Mean ± SD	28.1 ± 1.4	27.5 ± 1.1	27.4 ± 1.3
Range [min/max]	26/30	26/30	26/30

Volunteers ≤ 39 years of age were classified as young adults; volunteers who were ≥ 60 years were classified as old adults, and those between 40 and 59 years of age were classified as middle-aged adults. These age splits were based on our earlier volumetric work (Malykhin et al. 2017)

6 key areas: memory, orientation, judgment and problem solving, community affairs, home and hobbies, and personal care. A composite score from 0 to 3 was calculated. All of our participants met the cutoff score of < 0.5 for the total CDR score. To screen older volunteers for depression, the Geriatric Depression Scale was used (Yesavage et al. 1982). Designed to rate depression in the elderly, a score of > 5 is suggestive of depression, and a score > 10 is indicative of depression. All of our elderly (> 50 years of age) participants had a score of 4 or lower. Lastly, all older (> 50 years of age) participants were assessed for vascular dementia with the Hachinski Ischemic Scale (HIS; Hachinski et al. 1975). A score above 7 out of 18 has 89% sensitivity. HIS scores of all elderly participants were 3 or lower. Written informed consent was obtained from each participant, and the study was approved by the University of Alberta Health Research Ethics Board.

Data acquisition

All images were acquired on a 4.7 T Varian Inova MRI scanner at the Peter S. Allen MR Research Centre (University of Alberta, Edmonton, AB) using a single-transmit volume head coil (XL Resonance) with a 4-channel receiver coil (Pulseteq). 200 functional volumes were collected axially (in parallel to the AC–PC line) using a custom-written T_2*-sensitive Gradient Echo Planar Imaging (EPI) pulse sequence sensitive to blood oxygenation level-dependent (BOLD) contrast [repetition time (TR): 3000 ms; echo time (TE): 19 ms; flip angle: 90°; field of view (FOV): 216 × 204 mm^2; voxel size: 3 × 3 × 3 mm^3; 45 interleaved slices; phase encoding direction: anterior to posterior; GRAPPA parallel imaging with acceleration factor 2 (Griswold et al. 2002)]. For the resting-state portion of the scan, subjects were instructed to remain still, stay awake, and keep their eyes closed. To estimate B_0 inhomogeneity, two gradient echo images with different echo times were acquired with coverage and resolution matching those of the functional MRI data [TR: 500 ms; TE1: 4.52 ms; TE2: 6.53 ms; flip angle: 50°; FOV: 216 × 204 mm^2; voxel size: 3 × 3 × 3 mm^3; 45 interleaved slices]. A whole-brain T_1-weighted 3D Magnetization Prepared Rapid Gradient Echo (MPRAGE) sequence [TR: 8.5 ms; TE: 4.5 ms; inversion time: 300 ms; flip angle: 10°; FOV: 256 × 200 × 180 mm^3; voxel size: 1 × 1 × 1 mm^3] was used to acquire anatomical images for tissue segmentation and registration to standard space.

Image preprocessing

Functional images were processed using SPM12 (Wellcome Trust Centre for Neuroimaging, UCL, UK), FSL (Jenkinson et al. 2002; Smith et al. 2004), and ANTS (Avants and Gee 2004; Avants et al. 2008) software packages. Prior to registration, MPRAGE images underwent correction for intensity non-uniformity using N3 (Sled et al. 1998) and SPM12 bias correction algorithms. Subsequently, each participant's structural images were segmented into tissue probability maps using SPM12 unified segmentation.

Functional data were preprocessed with a series of steps commonly used in the field (Fig. 1a). The first four functional volumes of each dataset were discarded to ensure T_1-equilibrium. SPM12 FieldMap toolbox was used to estimate B_0 distortions and to generate voxel displacement maps caused by B_0 inhomogeneity. The unified '*realign & unwarp*' function in SPM12 was then used to correct geometric distortions in the fMRI data and to realign all fMRI volumes to the first functional volume (SPM12; Andersson et al. 2001). Following the realignment procedure, fMRI images underwent correction for slice acquisition-dependent time shifts. To ensure optimal tissue alignment between the anatomical and functional data, fMRI datasets were registered to matching T_1-weighted anatomical scans using boundary-based registration (FSL; Greve and Fischl 2009). To register RS-fMRI data to the MNI template, the SyN algorithm (ANTS; Avants et al. 2008) was used to compute tissue deformation fields based on T_1-weighted structural data. Normalized fMRI datasets were resampled to a 2 × 2 × 2 mm^3 voxel size and smoothed with a 6-mm FWHM Gaussian kernel (SPM12; Wellcome Trust Center for Neuroimaging, UCL, UK).

Manual labeling of subject-level independent components

We employed Probabilistic Independent Component Analysis with an automated estimation of the number of independent components (FSL; Beckmann & Smith, 2004) to remove motion-related, cardiovascular, and respiratory signals from our RS-fMRI data. ICA-based fMRI denoising strategies have two major advantages over scrubbing and spike regression approaches: (1) they preserve autocorrelation properties of the RS-fMRI signal, and (2) they are able to capture complex interactions between various noise sources (Pruim et al. 2015a). Since no other studies have performed noise component labeling on our 4.7 T Varian scanner, we performed manual identification of noise components in every subject. Building an automated classifier for ICA-based (e.g., FIX classifier; Salimi-Khorshidi et al. 2014) denoising using the current dataset was not feasible, as it would have necessitated removing subjects from our sample of 105 individuals to train a brand new classifier, reducing the study sample size.

Consequently, a single rater (SH) labeled all components as (1) potential resting-state network or (2) noise based on the criteria outlined in Griffanti et al. (2017). As advised by Pruim et al. (2017), only unambiguous noise components

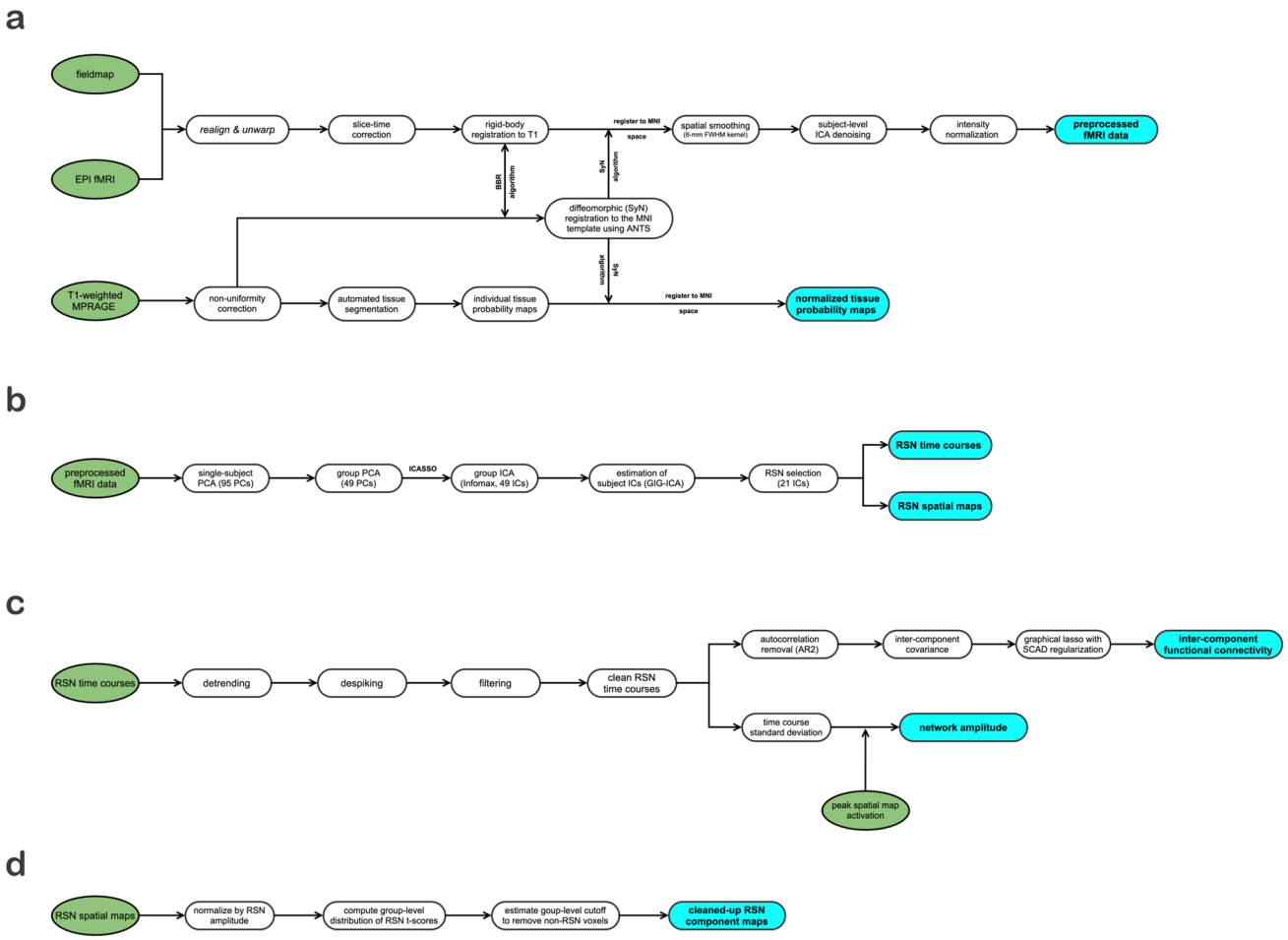

Fig. 1 Overview of image-processing pipeline. **a** Preprocessing of structural and functional data prior to group ICA decomposition; **b** fMRI decomposition into constituent signal sources using group ICA; **c** postprocessing of network time courses; **d** postprocessing of network spatial maps. Green, pipeline input; cyan, pipeline output. Outputs of panels **c** and **d** were used to study brain aging

were labeled for removal. To this end, spatial maps, time courses, and power spectra of every component were manually inspected. First, eye ghosting, scanner noise, cardiovascular, and respiratory components were identified by manual inspection. Components labeled as scanner noise were identified by two criteria: (1) majority of spatial activation outside the gray matter, and (2) distinct power spectrum pattern, dominated by high-frequency spikes—generally above 0.11 Hz—with little to no power represented by lower frequencies (i.e., < 0.10 Hz). Cardiovascular and respiratory noise sources were identified based on Griffanti et al. (2017) guidelines, while head motion artifacts were identified using Griffanti et al. (2017) criteria with the aid of a fully automated head motion component classifier ICA-AROMA (Pruim et al. 2015a).

Inter-rater and intra-rater reliabilities for component classification were performed on 100 components, chosen semi-randomly from 16 subjects. This reliability set consisted of 50 'noise' and 50 'signal/unclear' ICs, based on a prior (1 month earlier) classification by SH. The intra-rater reliability was assessed by SH, who classified those 100 ICs into 'remove'/'retain' categories twice, with a 2-week interval between each classification. The 'remove'/'retain' inter-rater reliability was assessed by two independent analysts—SH and NVM. Intra-rater and inter-rater Dice Similarity Coefficients (DSCs) for 'remove'/'retain' categories were 0.93/0.93 and 0.92/0.91, respectively. Thus, our manual component labeling showed a high degree of consistency, with more than 9 out of 10 ICs receiving identical labels in intra-observer and inter-observer evaluations.

Eye ghosting and dominant head motion artifacts (e.g., global signal drifts with spatial maps localized exclusively to the skull) were removed using the 'aggressive' option in *fsl_regfilt*, while all other artifacts were removed using the 'soft' regression option in *fsl_regfilt* (Beckmann and Smith 2004; Griffanti et al. 2014). Griffanti et al. (2014) demonstrated that 'soft' regression produces a good data cleanup

without sacrificing network signals. Consequently, this was our primary approach for noise removal.

Lastly, prior to running the group ICA decomposition, each subject's denoised RS-fMRI dataset was intensity normalized (Fig. 1a). Intensity normalization has been previously shown to improve the test–retest reliability of group-level ICA decompositions (Allen et al. 2010). It also ensures that resting-state BOLD signal fluctuations in every subject are scaled to % signal change units.

Group independent component analysis

Recent FC studies revealed that there are multiple regions in the human brain that participate in more than one RSN, primarily in the frontal and parietal association cortices (Liao et al. 2017; Mueller et al. 2013; Yeo et al. 2014). Group ICA (GICA; Calhoun et al. 2001) with a newer generation of subject-level reconstruction techniques can capture many of these FC complexities (Allen et al. 2012; Du et al. 2017; Yeo et al. 2014), while also foregoing the need to make somewhat arbitrary choices about which seeds/atlases one ought to use in connectivity comparisons. Here, we used the GIFT toolbox for MATLAB to perform group-level data-driven network decomposition (Calhoun et al. 2001; http://icatb.sourceforge.net/groupica.htm). Below, we outline detailed choices of the parameters we used in our decompositions (see Fig. 1b for flow-chart form).

Since our RS-fMRI data underwent substantial denoising at the individual level, resulting in reduced source dimensionality, we chose not to set the ICA model order based on previously published literature. Instead, we estimated model order by running the Infomax ICA algorithm (Bell and Sejnoski 1995) 200 times in ICASSO (http://www.cis.hut.fi/projects/ica/icasso). This approach renders Independent Component estimation insensitive to initial search parameters of the ICA algorithm, and directly estimates component reliability for each model order (Himberg et al. 2004). The ICASSO implementation in the GIFT toolbox provides quality estimates for all component clusters via the intra-cluster and extra-cluster similarity index, *Iq*. Our goal was to find the ICA model order such that *Iq* for all component clusters was 0.80 or higher, which resulted in 49 components. The initial subject-specific principal component analysis (PCA) retained 95 principal components (PCs) using standard decomposition. On average, 95 PCs explained 92.3% (range: 87.7–99.7, SD = 1.99) of variance in each preprocessed subject-specific fMRI dataset, while providing some data compression to reduce the computational demands. We used group-information guided ICA (GIG-ICA; Du and Fan 2013), which uses group-level ICs to guide subject-level ICA, for computing subject-level ICs and time courses (Fig. 1b). Inter-individual differences in network structure exist (Gordon et al. 2017; Laumann et al. 2015), and GIG-ICA is better positioned to capture those inter-individidual differences than back-reconstruction or dual regression (Du et al. 2016).

Group-level RSN ICs were identified by two viewers (SH and NVM) who manually inspected the aggregate spatial maps and power spectra. Specifically, when evaluating the average power spectra, two well-established metrics were used: (1) dynamic range, and (2) low frequency to high-frequency power ratio [for details see, Allen et al. (2011) and Robinson et al. (2009)]. We employed a relatively conservative labeling scheme, whereby only components resembling previously identified networks (Allen et al. 2011; Power et al. 2011; Yeo et al. 2011) were classified as RSNs. Given our set of criteria, we successfully identified 21 RSN ICs [subsequently termed *network components* or simply *RSNs*].

Subject-specific network time courses were detrended (involving removal of the mean, slope, and period π and 2π sines and cosines over each time course) using the multi-taper approach (Mitra and Bokil 2008) with the time-bandwidth product set to 3 and the number of tapers set to 5 (Fig. 1c). The RSN spatial maps were thresholded to ensure that our analyses were focused on the subset of voxels, which are most consistently associated with the network time courses across all subjects in our sample (Fig. 1d). Thresholding was based on the distribution of voxelwise *t*-scores using a model-based approach outlined in Allen et al. (2011). According to this model, the distribution of voxelwise *t*-statistic scores can be approximated by a linear combination of 1 normal and 2 gamma functions (Suppl. Figure 1). The normal distribution represents network-irrelevant voxels, while the two gamma functions represent positive and negative network sources (i.e., areas positively and negatively correlated with the network's time course). Mathematically, this relationship is explained by Eq. 1:

$$\begin{aligned} \boldsymbol{t} \approx\ & p_{c1}N\left(t_c|\mu_c,\sigma_c\right) + p_{c2}G\left(\boldsymbol{t}_c - \mu_c|\alpha_{c1},\beta_{c1}\right) \\ & + \left(1 - p_{c1} - p_{c2}\right)G\left(-\boldsymbol{t}_c - \mu_c|\alpha_{c2},\beta_{c2}\right). \end{aligned} \tag{1}$$

Values of the six parameters (μ_c, σ_c, α_{c1}, β_{c1}, α_{c2}, and β_{c2}) were estimated by minimizing the root-mean-squared-deviation (RMSD) between the modeled and empirical **t**-statistic distributions using the SIMPLEX algorithm (Nelder and Mead 1965). To ensure that the optimal global solution was obtained, the optimization algorithm was initiated 15,000 times, each time with a different set of randomly chosen values. The most relevant solutions for thresholding purposes are μ_c and σ_c parameters of the normal distribution, as the normal distribution represents network-irrelevant voxels. Here, we thresholded our spatial maps at $\mathbf{t} \geq \mu_c + 3\sigma_c$. We found this threshold to be a good compromise between sensitivity and specificity: in all networks, $\mathbf{t} \geq \mu_c + 3\sigma_c$ threshold was stricter than False Discovery Rate (FDR) $q < 0.05$ and stricter than FDR $q < 0.01$ in 8 RSNs, while, on average,

56% of RSN-related voxels were retained. All subsequent mentions of component topography and intra-network FC refer to thresholded ICs.

Since Allen et al. (2012) demonstrated that in the presence of spatial variability, network amplitude is best captured as a product of time course standard deviation and peak spatial map intensity (here, the average intensity value of the top 1% of IC's voxels), we used this measure as a proxy for RSN amplitude. Due to the pre-ICA intensity normalization, the resulting amplitude values were (approximately) in percent signal change units. To ensure that IC spatial maps represent only network topography, as opposed to topography + activation, we normalized all RSN spatial maps by network amplitude (Allen et al. 2011). Network components were visualized using open-source Visualization Toolkit software (VTK; Schroeder et al. 2006).

Modeling age relationships for network amplitude

To build models for each RSN's amplitude's relationship to age, we relied on the fractional polynomial [polynomial set: age^{-2}, age^{-1}, $age^{-0.5}$, ln(age), age^{1}, age^{2}, age^{3}] framework (Royston and Altman 1994; Sauerbrei and Royston 1999; Sauerbrei et al. 2006). The fractional polynomial (FP) technique controls for overfitting by restricting shape complexity if a model with $k+1$ powers does not produce a statistically better fit than a model with k powers.

Since the residual normality and residual homoscedasticity assumptions of the OLS estimator were violated in our RSN amplitude data (see Suppl. Table 1), we used L_1 (i.e., least absolute deviation), as opposed to L_2 (i.e., least squares), regressions to estimate the aging trajectories. Unlike L_2 models, which build trajectories to explain the population mean, L_1 regressions produce fits that explain the population median and are more robust to heteroscedastic, highly skewed data with severe outliers (Dielman, 2005; Lawrence and Shier 1981; Wimble et al. 2016). Custom-written MATLAB scripts employing the SIMPLEX algorithm (Nelder and Mead 1965) were used to find optimal L_1 trajectories.

Statistical significance tests were performed sequentially: (1) best-fitting FP2 (i.e., fractional polynomial model with 2 age power terms) vs. best-fitting FP1, (2) best-fitting FP1 (i.e., fractional polynomial model with 1 non-linear age power term) vs. linear, (3) linear vs. constant. The test statistic that we used to evaluate all L_1 regressions was

$$F_{\mathrm{LAD}} = \frac{2\left(\mathrm{SAR}_{\mathrm{reduced}} - \mathrm{SAR}_{\mathrm{full}}\right)}{\hat{\tau}}, \tag{2}$$

where $\mathrm{SAR}_{\mathrm{reduced}}$ and $\mathrm{SAR}_{\mathrm{full}}$ represent the sum of absolute values of the residuals for the reduced and full models, respectively. The denominator parameter τ is the L_1 estimate of residual variability for the full model (for more details on L_1 significance testing, see Birkes and Dodge 1993). To estimate F_{LAD} distributions under each null hypothesis, we performed Monte Carlo simulations (Suppl. Figure 2), using a conceptual framework that is similar to Freedman and Lane's (1983) permutation tests for L_2 regressions. Consistent with the Freedman and Lane (1983) approach, we treated our sample's L_1 regression coefficients as proxies of the true population-level relationship. For each significance test, we first estimated L_1 residuals for the reduced model. However, rather than permuting those residuals (the assumption of residual exchangeability was severely violated in our data; see Suppl. Table 2), we first split each network component's L_1 residuals into 3 age groups: young adult [$N=43$; age range: 18–39 years, mean = 27.1 years], middle-aged [$N=31$; age range: 41–59 years, mean = 50.0 years], and old adult [$N=31$; age range: 61–85 years, mean = 70.3 years]. Each age group's residuals were then used to estimate (using MATLAB's *ksdensity* function) separate residual distributions for young, middle-aged, and old adults (see Suppl. Figure 2 for examples). Those distributions were subsequently bias-corrected to ensure that the average median of each distribution was centered at 0. In residual simulations, if an individual's age was under 27 years of age, all residuals were randomly sampled from the 'young' distribution exclusively. Similarly, for every individual above 70 years of age, residuals were randomly sampled from the 'old' distribution exclusively. For individuals between 27 and 70 years of age, sampling was performed probabilistically from the two distributions closest to a given subject's age with weights varying as a linear function of age (e.g., residuals for a 60-year-old had a 50/50% chance of being sampled from the 'middle-aged' or 'old' distribution; residuals for a 65-year-old had a 25/75% chance of being sampled from the 'middle-aged'/'old' distribution, respectively). Such probabilistic sampling smoothed out transitions between age groups by blending the neighboring residual distributions. Lastly, our simulated residuals were added to the previously estimated null hypothesis (i.e., reduced) model, generating one null hypothesis dataset. Each of our F_{LAD} distributions was constructed from 25,000 such simulations (see Suppl. Figure 2 for a flow-chart example of linear vs. FP1 model comparison). System-level Holm–Bonferroni correction for multiple comparisons was applied for FP-selected vs. null (i.e., constant) model comparisons [3 comparisons for the somatomotor system, 4 comparisons for the visual system, 1 comparison for the auditory system, 6 comparisons for the default system, 1 comparison for the dorsal attention system, 2 comparisons for the executive control system, and 4 comparisons for the multi-system/mixed components].

Due to sampling-related uncertainty, model choice in data-driven model selection can vary from one dataset to the next. To minimize the effects of model selection uncertainty,

we performed weighted model averaging for all of our non-linear fits. Model averaging was performed on a subset of all plausible regression shapes, up to the last statistically significant FP order. Since our RSN amplitude datasets did not satisfy the criteria of theory-driven model averaging, we used bootstrap model selection frequencies as proxies for model selection uncertainty (for an overview of model averaging, see Burnham and Anderson 2002). Bootstrap model averaging was done iteratively. First, a crude model-averaged fit was estimated using paired bootstrap sampling (100 samples). For each paired bootstrap sample, the model with the smallest sum of absolute error terms was selected using a repeated (50 times) 20-fold cross-validation. Next, estimates of model selection uncertainty were refined by bootstrapping that average fit's residuals. To preserve age-specific residual properties (same issues as L_1 hypothesis testing), all bootstrap samples of the residuals were performed in an age-restricted manner (SD = 3 years, relative to each subject's age). During this refined estimation of model selection uncertainty, 500 bootstrap samples were taken, and the model with the smallest sum of absolute error terms was chosen as the best model for each bootstrap sample using a repeated (100 times) 20-fold cross-validation. These refined model selection frequencies were used to compute the final model-averaged fits for all non-linear (i.e., FP1 and FP2) models.

To verify our L_1 regression results, we also performed amplitude comparisons among the three major age groups [young: under 40 years (mean age = 27.1 years); middle: 40–59 years (mean age = 50.0 years); old: 60 years and older (mean age = 70.3 years)]. A bias-corrected bootstrap test for statistical significance (50,000 samples) on the difference of age group medians was used for statistical inference. Significance was declared when the FWE 95% bias-corrected accelerated (BCa) confidence interval (CI) excluded zero. System-specific (as above) Holm–Bonferroni correction for multiple comparisons were carried out sequentially. Initially, we tested the significance of group comparisons with the largest amplitude differentials (typically young vs. old) among all RSNs of a brain system (e.g., visual, default, somatomotor, etc.). If statistically significant, follow-up Holm–Bonferroni-corrected comparisons [3 tests: (1) young vs. middle, (2) middle vs. old, and (3) young vs. old] were performed to determine whether network amplitude differed in the other age group comparisons.

Modeling age relationships for spatial maps

Permutation-based *F*-tests (50,000 permutations using FSL's *randomize* function with threshold-free cluster enhancement option; Smith and Nichols 2009) were used to test for the presence of linear or quadratic relationships to age in component topography. Clusters with statistically significant relationships to age were cleaned up by (1) removing all clusters with volumes smaller than 80 mm^3, representing 1–3 native space voxels, (2) removing all clusters dominated (i.e., 50% or more) by white matter (WM) or cerebrospinal fluid (CSF) signal, and (3) removing clusters, in which gray matter contribution to the cluster peak (top 30% of voxels with the strongest association to age) was less than 50%. All age clusters that survived this cleanup procedure were followed up with parametric fractional polynomial regression (RA2 model selection; Ambler and Royston 2001). Similar to RSN amplitude methodology, if non-linearity tests were significant, bootstrapping was used to account for model selection uncertainty by building model-averaged fits.

Finally, because it is well established that cortical gray matter (GM) volume is negatively correlated with age (Good et al. 2001; Fjell et al. 2009a; Raz et al. 1997, 2004, 2005), we examined whether adding a cluster's GM volume would eliminate statistical association to age in spatial map regions showing age effects. To answer this question, we performed cluster-level regressions (i.e., RSN signal averaged across a cluster) with subject age and local GM density as the independent variables. Significant regression coefficients for age are indicative of age-related differences in network topography that cannot be fully accounted for by age-related changes in regional GM volume. Our GM density maps were estimated in native space using SPM12 automated tissue segmentation pipeline and were subsequently registered to the MNI template using the same transformation matrices that we used for normalizing our fMRI data.

Between-component connectivity

The most common approach to building graphical models of brain organization is to use time course correlation coefficients as proxies for FC (Craddock et al. 2013; Smith et al. 2011). However, this approach suffers from two significant limitations: (1) a lack of control for communication via indirect paths (Epskamp and Fried 2018; Smith et al. 2011; Zhu and Cribben 2018), and (2) a reliance on somewhat arbitrary thresholding (van den Heuvel et al. 2017; van Wijk et al. 2010). To avoid these issues, we used a sparse precision matrix estimation procedure in our inter-IC FC analyses. Sparse estimation methods shrink spurious or indirect connections to 0 by penalizing excessive model complexity if there is insufficient evidence in the data to support a complex connectome (Smith et al. 2011; Zhu and Cribben 2018).

Zhu and Cribben (2018) used simulations to show that sparse network structure is best recovered using the maximum likelihood estimation of the precision matrix with the smoothly clipped absolute deviation (SCAD) regularization term as a penalty for model complexity. This approach belongs to a family of graph estimation techniques building on the graphical lasso framework (Friedman et al. 2008).

Similar to the graphical lasso, incorporating the SCAD regularization term during graph estimation allows for the optimal balance between network complexity and network likelihood; however, relative to the more common LASSO penalty term, using SCAD reduces bias without sacrificing model stability (Fan and Li 2001; Zhu and Cribben 2018). The SCAD penalty relies on two tuning parameters, a and ρ. To minimize the Bayes risk, Fan and Li (2001) recommend $a = 3.7$. The second tuning parameter, ρ, was selected using Bayesian Information Criterion (BIC) from a set of $\rho i = i \times 0.01$, with $i = 1, 2, 3 \ldots, 100$. The ρ with the lowest BIC value was used to build final graphs (Fan et al. 2009; Zhu and Cribben 2018). Since temporal autocorrelation in the fMRI time series can produce biased FC estimates (Arbabshirani et al. 2014; Zhu and Cribben 2018), each component's time course was whitened (using AR2 model) prior to graph estimation. Furthermore, since averaging across subjects improves the stability of edge detection when using sparse graphical methods, inter-component FC was estimated on group-averaged (i.e., young, middle-aged, and old adults) covariance matrices. For reasons detailed in Rubinov and Sporns (2010), edges representing anti-correlations were removed from the estimated graphs. All sparse graphs were estimated using custom-written *R* functions, and Gephi (v0.9.2; Bastian et al. 2009) was used for graph visualizations. Follow-up graph summary metrics were computed using freely available Brain Connectivity Toolbox for MATLAB (Rubinov and Sporns 2010).

Since our inter-component FC was estimated at the group level, we relied on group comparisons [Young vs. Old, Young vs. Middle, Middle vs. Old], rather than on correlation-based methods, to study age differences in inter-component FC. Edge weight comparisons and weighted graph summary metrics were used to study age effects on FC strength, while unweighted graph summary metrics were used to study age differences in graph architecture, independent of FC strength. Mathematical definitions of all weighted and unweighted graph summary metrics that were used in this study are provided in the Supplementary Materials.

Statistical significance for each graph-based age comparison was assessed using permutation tests (10,000 permutations), and false discovery rate (FDR)-corrected results are reported, for $q = 0.05$ (Hochberg, 1988). Global graph summary metrics were corrected for 3 tests (i.e., Young vs. Old, Young vs. Middle, Middle vs. Old), node centrality metrics for 21 tests (i.e., 21 RSNs in each age comparison), and edge comparisons for 56–59 tests (depending on the number of non-zero edges in relevant age groups). Since this study was exploratory in nature, we also report edge weight differences that survived an uncorrected $p < 0.01$ threshold.

Results

Resting-state brain networks and their functional connectivity profiles

Following group-level spatial ICA decomposition, we identified 21 ICs representing RSN sources: 3 somatomotor [SM1, SM3, and SM3], 4 visual [Vis1, Vis2, Vis3, and Vis4], 1 auditory [Au], 6 default mode [DM1, DM2, …, DM6], 1 dorsal attention [DA], 2 executive control [EC1, EC2], and 4 ICs with spatial maps covering multiple brain systems, according to the Yeo et al. (2011) functional parcellation of the cerebral cortex. We termed those multi-system ICs as mixed RSNs [Mix1–Mix4]. Figure 2 demonstrates the spatial topography of each network component in our study (see Suppl. Figures 3, 4, 5, 6 for additional views).

Consistent with the underlying physiology, our somatomotor RSNs corresponded to face, hand, and leg areas of the primary somatosensory and primary motor cortices. Similarly, our visual ICs represented central/peripheral and primary/secondary visual processing pathways, while the default system was split into the dorsal medial (DM3 and DM6), medial temporal (DM2), and core (DM1, DM4, and DM5) subsystems. Although 3 default mode subsystems are typically emphasized in the literature (Andrews-Hanna et al. 2010, 2014; Christoff et al. 2016), using 4.7 T data, we obtained a more refined splitting of the DMN into its sub-components. RSNs of other cognitive systems, namely the dorsal attention and executive control, were captured by relatively few ICs (Fig. 2).

Our SCAD-regularized FC graph, representing direct inter-component FC for the entire (i.e., age-averaged) sample, revealed a high degree of functional specialization in the somatomotor and visual areas with few direct connections to other functional systems (Fig. 3). This is in contrast to the default, dorsal attention, and executive control RSNs, which demonstrated a high degree of interconnectedness with network components from other functional systems: DA, DM1, DM5, and EC2 RSNs each had 2 or more direct connections with systems other than their own. Most multi-system (i.e., mixed) network components served as bridge nodes connecting functionally segregated systems to each other (Fig. 3).

Network amplitude and age

Our L_1 regression analyses showed that signal amplitude in every RSN was negatively associated with age (all corrected ps < 0.05; Figs. 7, 8, 9). Non-linearity tests were statistically significant in only 4 out of 21 RSNs—SM2, SM3, Vis3, and DA—indicating that linear models provide a reasonable explanation of the association between age and BOLD signal amplitude in most brain areas. In a

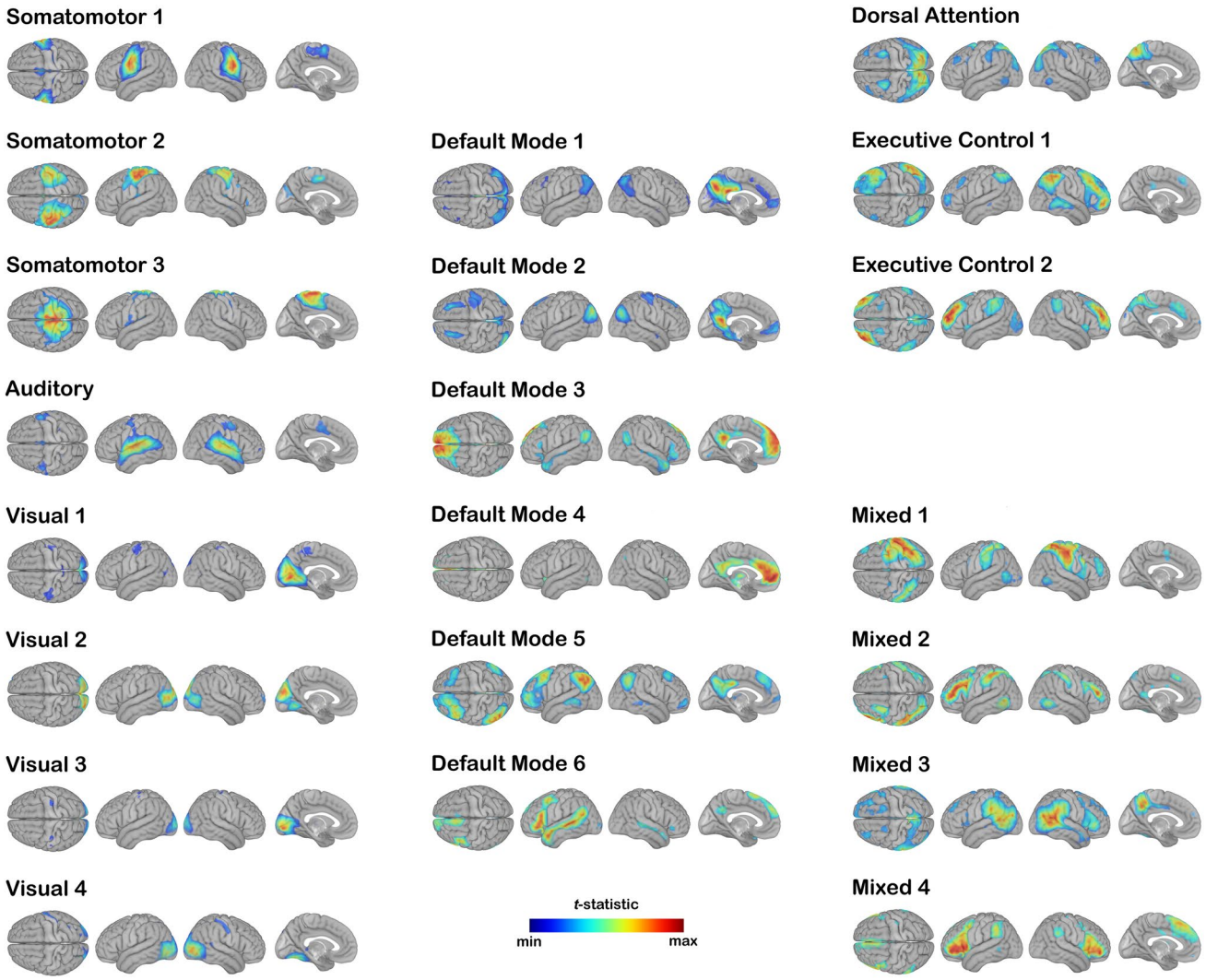

Fig. 2 Intrinsic network components identified by the group-level independent component analysis

typical 75-year-old, the system-averaged (i.e., averaged across 6 default mode components, 4 visual components, and 3 somatomotor components) BOLD signal amplitude was reduced by 61% in the somatomotor system, 63% in the visual system, 41% in the auditory system, 37% in the default system, 53% in the dorsal attention system, and 38% in the executive control system, when compared to a typical 25-year-old (Figs. 4, 5). The smallest (30% or less) age-associated decline of BOLD amplitude was observed in the default mode and Mix4 ICs (Fig. 5), while all of the somatomotor and visual ICs showed > 50% BOLD amplitude reduction from young adulthood to old age (Fig. 4).

To determine whether a common brain-wide process is responsible for the observed BOLD amplitude decline with age, we performed a principal component analysis (PCA) on the amplitude data from all network ICs. Only the first principal component, explaining 58% of the RSN amplitude variability, was statistically significant in this PCA decomposition. This principal component (Fig. 6) was positively correlated with every RSN (correlation coefficients between 0.545 and 0.865) and negatively correlated with age ($r = -0.553$, $p < 0.001$).

Age group comparisons of the RSN amplitude and amplitude variability were statistically significant in most young vs. old tests, with some networks also showing statistically significant differences in young vs. middle and/or middle vs. old comparisons (Suppl. Figures 7, 8, 9). However, unlike the continuous models, which showed age-associated decline of BOLD amplitude in every RSN, group amplitude comparisons did not detect any age differences in the DM2 and Mix4 network components. In all instances where young vs. old comparisons were statistically significant,

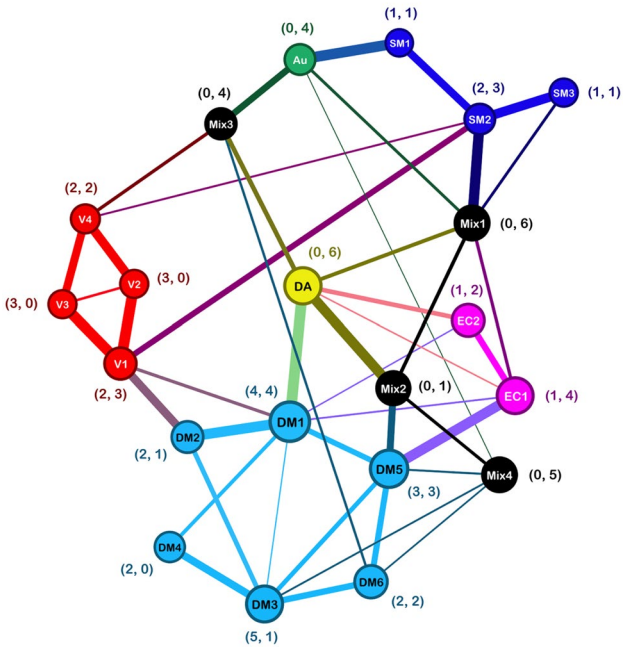

Fig. 3 Graphical representation of the intrinsic inter-component functional connectivity. Only positive correlations are shown. Edge thickness represents the magnitude of SCAD-regularized partial correlation for network component pairs. Node size represents the magnitude of unweighted eigenvector centrality. Coordinates depict the number of within-system (left number) and between-system (right number) connections. Node colors represent functional systems to which each network component belongs: SM, somatomotor (blue); V, visual (red); Au, auditory (green); DM, default mode (cyan); DA, dorsal attention (yellow); EC, executive control (magenta); Mix, mixed (black)

median RSN amplitude was larger in young adults than in middle-aged and old adults, and larger in middle-aged adults than in old adults, suggesting a continuous and progressive reduction in RSN signal amplitude throughout life. Lastly, old adults had significantly lower inter-individual BOLD amplitude variability in all sensorimotor (SM1-3, Vis1-4, and Au) ICs, two default mode ICs (DM2 and DM3), two attention (DA and EC1) ICs, and three mixed (Mix1-3) ICs [all corrected $ps < 0.05$; see Suppl. Table 1]. Six network components—DM1, DM4-6, Mix4, and EC2—showed no age differences in BOLD amplitude's inter-individual variability (all $ps > 0.1$).

Component topography and age

Across all network components, we identified 23 clusters with either linear or non-linear statistical relationships to age (Table 2; Figs. 7, 8, 9, 10). Age relationship clusters were present in 5 out of 8 sensorimotor ICs, 4 out of 6 default mode ICs, 2 out of 3 attention/control ICs, and 2 out of 4 mixed ICs, suggesting that age effect on RSNs' spatial map profiles is not limited to one particular functional system. Most of those age relationship clusters (19 out of 23) represented reduced intra-component FC among the elderly; however, a small number (4 out of 23), restricted to the DM1 and DA RSNs, showed areas with stronger intra-component FC in old age. With the exception of a few clusters, age relationships were linear.

The largest clusters, representing age differences in network topography, belonged to the Mix4 IC. Those two clusters (clusters V and W; Table 2) were located within the bilateral inferior frontal gyrus and bilateral orbitofrontal cortex [BA44–47], roughly corresponding to the Broca's area and nearby cortices. Participation of these brain areas in Mix4 RSN declined from moderate/high in young adults (normalized activation of 0.4 and higher) to weak (normalized activation < 0.4) in old adults, which is indicative of BA44–47 areas becoming increasingly disconnected from the rest of the network with age. Two other large clusters (1) cluster K, belonging to the DM4 RSN, and (2) cluster F, belonging to the Vis4 RSN, also showed a reduction in intra-component FC with age. Four clusters with the strongest association to age (i.e., largest absolute correlation with age) were clusters F, W, V, and C, belonging to the Vis1, Vis4, and Mix4 RSNs (Table 2). All 4 clusters showed negative linear relationships to age with correlation coefficients ranging between − 0.54 and − 0.58. Cluster C was localized within the left lingual, intracalcarine, and precuneus cortices, while cluster F's anatomy was restricted to the right fusiform gyrus (Table 2). Clusters V and W and their anatomical profiles were described above.

GM volume was negatively associated with age in 21 out of 23 clusters. However, adding regional GM volume as an extra variable to cluster-level age regressions did not eliminate age effects in 21 out of 23 clusters (Table 2), demonstrating that age differences in component structure were not driven solely by age effects on cortical GM. Despite these overall trends, it is important to note that adding local GM volume as a regressor of no-interest eliminated age effects in clusters A and L (SM1 and DM4 RSNs, respectively). Together, these observations indicate that age differences in component topography are partially driven by age differences in regional GM. Furthermore, since cluster GM volume and intra-component FC were statistically associated in 17 clusters (assessed using distance correlation with 50,000 permutation tests for significance), causal study designs are needed for an accurate estimation of the extent to which structural and functional changes in the aging brain produce age differences in network topography.

Inter-component functional connectivity and age

Lastly, we examined the effects of age on inter-component FC. First, we built sparse graphical representations of

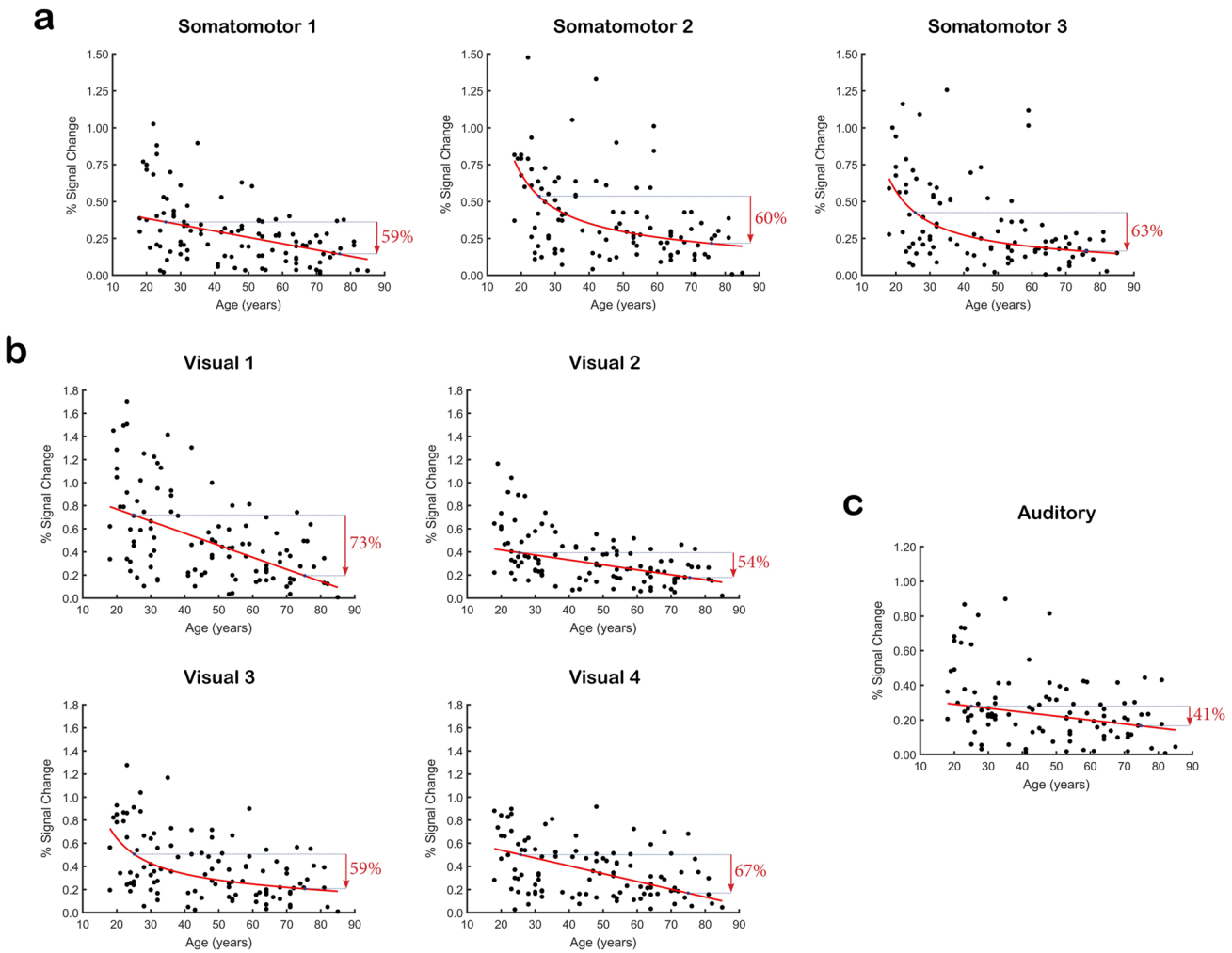

Fig. 4 L_1 fractional polynomial regression plots showing relationships between age and RS-fMRI amplitude in all **a** somatomotor, **b** visual, and **c** auditory networks. Red arrows represent relative differences in resting-state fluctuation amplitude between a median 25-year-old and a median 75-year-old

inter-IC communication for the young, middle-aged, and old adult groups. Those graphs are visualized in Fig. 11.

Descriptively, a core set of 31 connections was identified in every age group, suggesting that the overall pattern of the brain's functional organization did not differ drastically among age groups (Fig. 12). Most unweighted graph summary metrics, computed from binarized graphs, support this conclusion: global efficiency, transitivity, density, radius, diameter, characteristic path length, and centralization did not show any age-related statistical differences [all qs > 0.10, see Table 3 for details; see Suppl. Materials for mathematical definitions]. The only unweighted summary metric that attained statistical significance in our age comparisons was the number of intra-system connections. Specifically, the young adult group had fewer intra-system connections (a total of 15 edges) than middle-aged or old adult groups (a total of 19 edges in each group) [both qs < 0.05]. Despite differences in the number of intra-system connections, age groups did not show any statistical differences in the number of inter-system connections [all uncorrected ps > 0.10, see Table 3 for details].

Contrary to results from binarized graphs, we observed substantial age differences if weighted graphs were used to compute graph summary metrics (Table 3; see Suppl. Materials for mathematical definitions of weighted vs. unweigted graph summary metrics). The average edge thickness of all non-zero positive edges was greater in the young adult group than in the old adult group [$M_{\text{diff}} = 0.055$, $q < 0.010$], and greater in the young adult group than in the middle-aged group [$M_{\text{diff}} = 0.0424$, $q < 0.050$]. However, the average edge thickness of the middle-aged group did not differ from that of the old adult group [uncorrected $p > 0.10$], suggesting that inter-IC partial correlation strength declines with age and that this decline is more pronounced in early aging.

Furthermore, the aforementioned age differences in edge weight were driven by intra-system, not inter-system, connections (Table 3). Our age comparisons of weighted efficiency metrics—global efficiency, network radius, network diameter, and characteristic path length—revealed a gradual loss of connectivity efficiency with age [$\text{efficiency}_{\text{young}} > \text{efficiency}_{\text{middle}} > \text{efficiency}_{\text{old}}$; for details, see Table 3].

Next, we investigated node centrality to determine whether there were any age differences in component importance to the rest of the connectome. Similar to the unweighted global metrics, the unweighted degree, closeness, and betweenness centralities did not show any statistically significant age differences [all qs > 0.10, see Suppl. Table 2]. For the unweighted eigenvector centrality, we observed one statistically significant age effect in the Mix2 RSN: lower centrality in old relative to young adults [$\text{EigenCentrality}_{\text{young}} = 0.9705$, $\text{EigenCentrality}_{\text{old}} = 0.405$, $q \approx 0.050$]. Unlike its unweighted counterpart, weighted closeness centrality was reduced in old relative to young adults in all 21 RSNs (Table 4). Age differences in weighted degree and/or eigenvector centrality were found in SM2, Vis1, Au, DM1, DM2, DM6, DA, EC2, Mix1, Mix2, and Mix4 RSNs (see Table 4 for details), while weighted betweenness centrality did not show any statistically significant age effects. Taken together, these results demonstrate that the aging process modulates FC strength but does not lead to a substantial restructuring of the brain's functional architecture.

To determine which edges were most responsible for age differences in weighted global summary metrics and weighted node centralities, we performed age comparisons of FC strength on each non-zero edge in our graphs. After correcting for multiple hypothesis testing (FDR < 0.05, 56–59 tests), age differences were found in young vs. old (5 edges: SM2 ↔ Mix1, DM6 ↔ Mix4, Au ↔ Mix1, EC1 ↔ EC2, EC2 ↔ Mix4) and young vs. middle-aged (3 edges: SM2 ↔ Mix1, EC2 ↔ Mix4, DM1 ↔ Mix3), but not in middle-aged vs. old comparisons (Fig. 13, Table 5). All but one (i.e., DM1 ↔ Mix3) differences in edge weight displayed a reduction in FC with age, and all but one (EC1 ↔ EC2) involved one of the multi-system 'Mixed' ICs. Lowering the statistical threshold to uncorrected $p < 0.01$ resulted in 8 additional edges showing age differences (Fig. 13, Table 5), more than half of which were in the middle-aged vs. old adult comparison.

Discussion

In the current study, we investigated age differences for three primary features in ICA-based RSN decompositions: network amplitude, spatial topography of network sources, and inter-component functional interactions. For RSN amplitude, our findings led to three main conclusions: (1) BOLD amplitude is negatively associated with age in all networks, and a single process might underly these global amplitude trends; (2) sensorimotor networks, and not frontal or parietal association networks, showed the steepest amplitude reduction with age; (3) compared to young adults, old adults showed reduced inter-individual variability in network amplitude. For RSN/component topography, age differences in network structure were modest, and except for a few clusters in the parietal association areas, represented reduced intra-network FC. Finally, our age comparisons of inter-component FC revealed a large degree of age invariance in inter-network interactions. Where present, age differences in inter-component FC were captured by weighted, as opposed to unweighted, graph summary metrics. Together, weighted graph summary metrics indicate weakened inter-system (e.g., visual ↔ default mode, somatomotor ↔ attention) communication in old age, driven by age differences in functional communication via 'Mixed' (or multi-system) network components. To our best knowledge, this is the first high-field RS-fMRI study to provide such a comprehensive overview of alterations in the human brain's functional architecture for the entire adult lifespan.

Network amplitude and age

Our results showed that healthy cognitive aging was associated with a reduction of BOLD signal amplitude in every brain system. These findings are consistent with two previous studies that also used ICA to study age effects on FC (Allen et al. 2011; Zonneveld et al. 2019). In the first study, Allen et al. (2011) showed that aging was associated with a widespread reduction in low-frequency BOLD signal power (< 0.15 Hz). However, Allen et al. (2011) focused predominantly on maturation and early aging, with 80% of their sample falling in the 13–30 age range, and only 7 (~ 1.2%) subjects older than 50 at the time of data collection. In the second study, Zonneveld et al. (2019) found that advanced age was associated with lower mean signal amplitude in most RSNs; however, the authors did not study the entire adulthood and sampled older adults exclusively.

In the current study, we demonstrated that the fMRI signal amplitude of most RSNs declines linearly throughout the entire adult lifespan. For network components with non-linear trajectories, our results suggest a rapid reduction of BOLD amplitude in young adulthood, followed by a more gradual decline in middle and old age. Such non-linear aging patterns are not in agreement with most structural imaging work, which tends to show rapid tissue deterioration in old, as opposed to young adults (Aghamohammadi-Sereshki et al. 2019; Lebel et al. 2010; Malykhin et al. 2017; Pietrasik et al. 2020; Raz et al. 2004, 2005, 2010). Furthermore, we demonstrated that a single source of variance could explain age differences in BOLD amplitude in most RSNs,

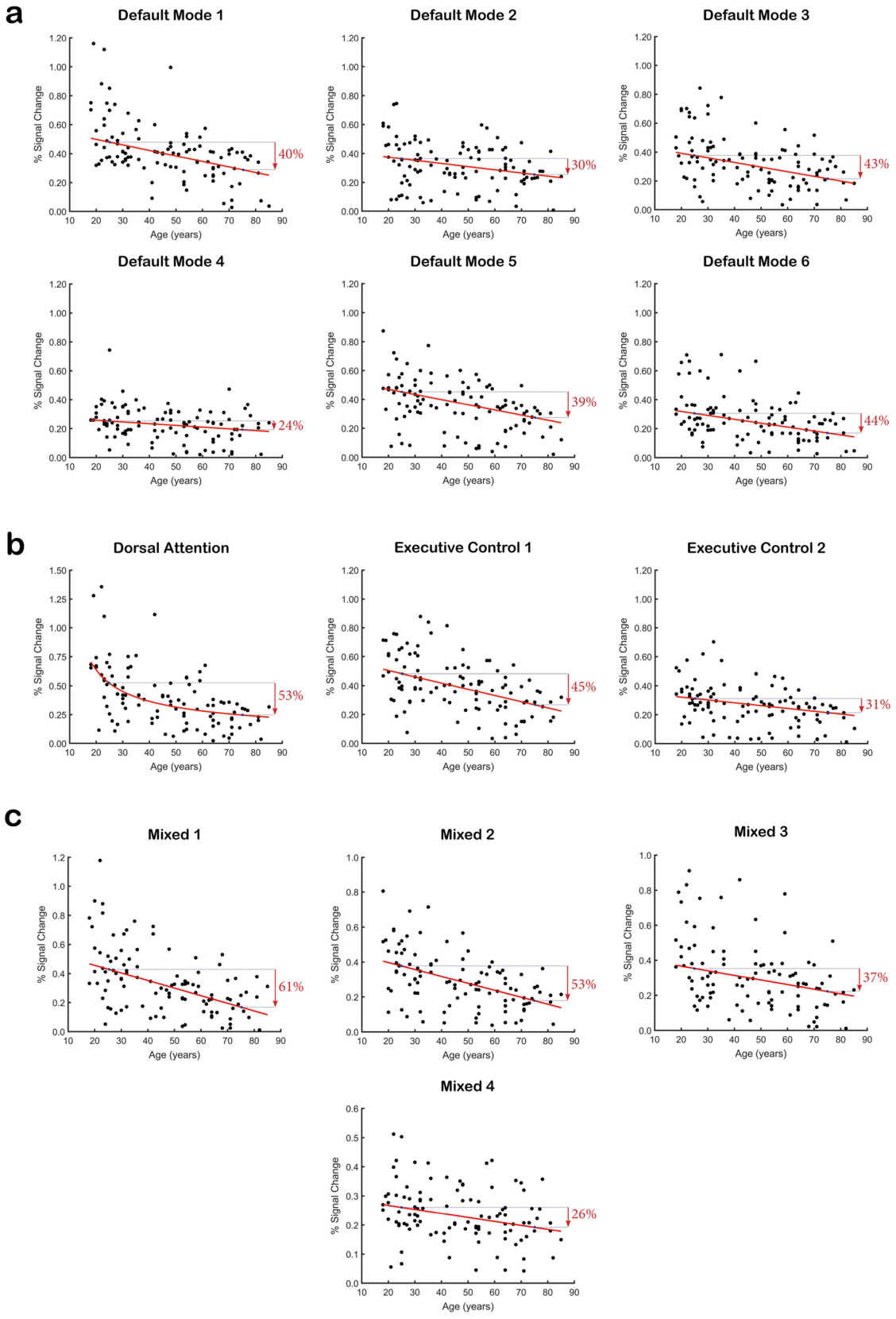
a
Default Mode 1
40%
Default Mode 2
30%
Default Mode 3
43%
Default Mode 4
24%
Default Mode 5
39%
Default Mode 6
44%
b
Dorsal Attention
53%
Executive Control 1
45%
Executive Control 2
31%
c
Mixed 1
61%
Mixed 2
53%
Mixed 3
37%
Mixed 4
26%
% Signal Change
Age (years)

◂**Fig. 5** L_1 fractional polynomial regression plots showing relationships between age and RS-fMRI amplitude in all **a** default, **b** attention-related, and **c** mixed components. Red arrows represent relative differences in resting-state fluctuation amplitude between a median 25-year-old and a median 75-year-old

suggesting that a common set of biological processes might be responsible for these BOLD amplitude effects. According to our results, the largest young vs. old amplitude differences were localized primarily within visual and somatomotor RSNs. Because previous structural imaging studies showed that GM in the primary sensorimotor regions is not as vulnerable to age-related atrophy as frontal GM (Fjell et al. 2009a, b; Leong et al. 2017; McDonald et al. 2009; Raz et al. 1997, 2004, 2005, 2010; Resnick et al. 2003), it is unlikely that cortical atrophy is the only cause of declining RSN amplitude in old age. Finally, we would like to point out that RSN amplitude among old adults was not only smaller but also had lower inter-individual variability.

Most previous studies on the relationship between BOLD amplitude and age were task based, and not resting-state (Cabeza et al. 2002, 2004; Grady et al. 1994; D'Esposito et al. 1999; Fabiani et al. 2014; Gutchess et al. 2005; Hesselmann et al. 2001; Hutchinson et al. 2002; Levine et al. 2000; Logan et al. 2002; Madden et al. 1996; Park et al. 2003, 2004; West et al. 2019). Experiments that employed motor paradigms to investigate age effects on the sensorimotor cortex reported: (1) smaller activation clusters in old adults (D'Esposito et al. 1999, 2003; Handwerker et al. 2007; Hesselmann et al. 2001; Mehagnoul-Schipper et al. 2002; Riecker et al. 2006); (2) age differences in BOLD response timing and BOLD response shape (Handwerker et al. 2007; Stefanova et al. 2013; Taoka et al. 1998; West et al. 2019); and (3) elevated noise levels among the elderly, relative to task-evoked activity (D'Esposito et al. 1999; Kannurpatti et al. 2011). In the visual system, a wide variety of task-based neuroimaging experiments revealed reduced BOLD activation (Grady et al. 1994; Fabiani et al. 2014; Ross et al. 1997; West et al. 2019; Wright and Wise 2018). These age effects were detected not only in fMRI experiments but also in Positron Emission Tomography (PET) and functional Near-Infrared Spectroscopy (fNIRS) studies, across a wide variety of visual paradigms, ranging from pure perception to face matching, working/episodic memory, and visual attention (Ances et al. 2009; Buckner et al. 2000; Cabeza et al. 2004; Fabiani et al. 2014; Grady et al. 1994; Handwerker et al. 2007; Hutchison et al. 2013; Levine et al. 2000; Li et al. 2015; Madden et al. 1996; Park et al. 2003; Rieck et al. 2015; Ross et al. 1997; Spreng et al. 2010; Ward et al. 2015; West et al. 2019). Age differences in activation amplitude were also identified in brain regions belonging to the default system (Grady et al. 2006; Lustig et al. 2003; Miller et al. 2008; Persson et al. 2007; Sambataro et al. 2010). However, the DMN's activity differences during task-based studies were reported as reduced or failed deactivation in old adults since the default system is more active at rest than during cognitively demanding tasks (Park and Reuter-Lorenz 2009; Persson et al. 2007, 2014; Raichle and Snyder 2007). The same biological changes might be responsible for amplitude differences in both resting-state and task-based fMRI research. This idea is supported by evidence from Yan et al. (2011), who showed that—at least in the visual cortex—the magnitude of RS-fMRI fluctuations was predictive of task-induced activation.

Each brain region's BOLD signal time course represents a complex interplay of four dynamic factors: local blood volume, rate of local blood flow, local vascular reactivity, and local rate of cerebral metabolic oxygen utilization ($CMRO_2$) (Cohen et al. 2004; Kim 2018; Kim and Ogawa 2012; Uludağ and Blinder 2018; Uludağ et al. 2009; Wright and Wise 2018). Reduced BOLD amplitude in old adults can be driven by lower cerebral blood flow (CBF), lower cerebrovascular reactivity (CVR), or higher $CMRO_2$. It is well documented that aging causes substantial changes in the cerebral vasculature, including stiffening of the vessel walls, reduction of the capillary density, and thickening of the capillary basement membrane (for reviews see, D'Espotio et al. 2003; Farkas and Luiten 2001; Wright and Wise 2018). In vivo work using PET and Arterial Spin Labeling (ASL) methods showed that aging individuals display lower CBF and lower CVR (Aanerud et al. 2012; Beason-Held et al. 2008; Bertsch et al. 2009; Chen et al. 2011; Galiano et al. 2019; Hutchison et al. 2013; Kety 1956; Liu et al. 2013; Lu et al. 2011; Melamed et al. 1980; Peng et al. 2014; Wright and Wise 2018; Yamaguchi et al. 1986). Consistent with our non-linear aging trajectories that suggest a steeper decline of BOLD amplitude from young to middle vs. middle to old adulthood, some studies reported a more rapid CBF decline in adolescents than in middle-aged or old adults (Biagi et al. 2007; Frackowiak et al. 1980; Zhang et al. 2017). Given such converging evidence, it is plausible that age effects on BOLD amplitude are driven by cardiovascular risk factors (Aanerud et al. 2012; D'Esposito et al. 2003; Farkas and Luiten 2001; Gagnon et al. 2015; Hillman, 2014; Kety et al. 1956; Liu 2013; Melamed et al. 1980; Zonneveld et al. 2019). For instance, a recent whole-brain RS-fMRI study by Zonneveld et al. (2019) reported a positive relationship between BOLD signal amplitude and systolic blood pressure, lending support to the notion that age effects on RSN amplitude are driven by cardiovascular risk factors (Aanerud et al. 2012; D'Esposito et al. 2003; Farkas and Luiten 2001; Gagnon et al. 2015; Hillman, 2014; Kety et al. 1956; Liu 2013; Melamed et al. 1980; Zonneveld et al. 2019). However, it is unlikely that age effects on our RSN amplitude measures were driven exclusively by age differences in blood pressure. Only 1 volunteer in our middle-aged cohort

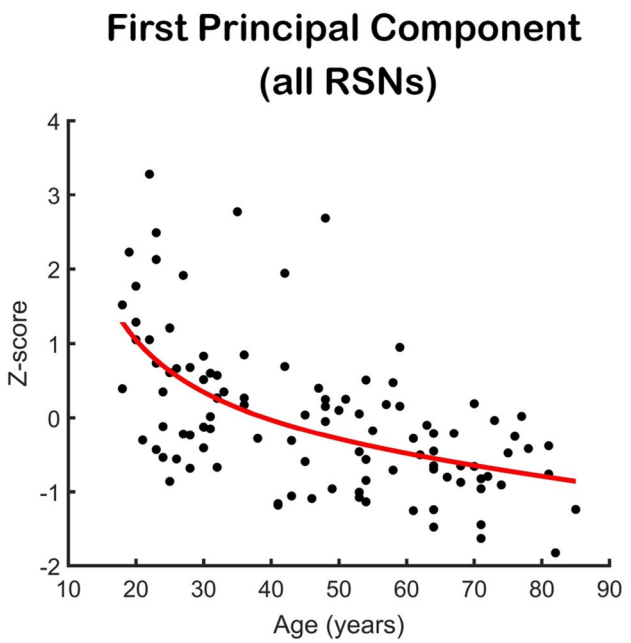

Fig. 6 Principal component representing amplitude variability common to all RSNs. Since aging trajectories for individuals RSNs were either linear or FP1 models, the age relationship trendline for this principal component is represented by a model-averaged fit of linear and FP1 L_1 regression models

had a history of elevated blood pressure, while the other 30 did not. Nonetheless, when compared to young adults, our middle-aged volunteers displayed lower group-level measures of RSN amplitude in multiple network components. Furthermore, a comparison of RSN amplitude between old adults with a history of high blood pressure to those without did not reveal any amplitude differences (all uncorrected $ps > 0.10$). It is worth noting, however, that only individuals with no history of high blood pressure or those whose high blood pressure was *controlled* by prescribed medications or lifestyle adjustments were recruited for our study. To what extent our RSN amplitude results might generalize to a broader population with a more severe history of cardiovascular disease is a topic that merits further research.

In addition to vascular factors, it is plausible that the aging process affects $CMRO_2$, modulating the oxy-/deoxyhemoglobin ratio in the regional cerebral vasculature, which in turn affects the fMRI-measured T_2^* contrast. Unlike CBF and CVR, $CMRO_2$ is a direct measure of neuronal metabolic demands (Cohen et al. 2004; D'Espotio et al. 2003; Kim 2018; Kim and Ogawa 2012; Uludağ and Blinder 2018; Wright and Wise 2018), and age differences in $CMRO_2$ likely represent differences in spiking rates and neurotransmitter trafficking (D'Espotio et al. 2003; Kim and Ogawa 2012; Logothetis et al. 2001). Unfortunately, human imaging literature is inconclusive on the direction of $CMRO_2$ changes in healthy aging: some studies (e.g., Aanerud et al. 2012) reported lower $CMRO_2$ in old adults, while others reported the opposite pattern (e.g., Lu et al. 2011; Peng et al. 2014). Additional research, employing quantitative high-resolution (1.8-mm isotropic or less) fMRI techniques, is needed to determine the exact cause of brain-wide age differences in RSN amplitude that were observed in the current work.

Functional connectivity and age

By combining GIG-ICA with sparse graphical methods, we demonstrated a substantial degree of age invariance in network architecture, a result that is in agreement with recent non-ICA-based RS-fMRI research (e.g., Chan et al. 2017; Grady et al. 2016; Han et al. 2018). Specifically, almost half of our network components displayed no age differences in component structure, and among the ones that did, age effects were captured by small (2% of IC volume, on average) regional clusters. Similarly, age comparisons of various unweighted graph summary metrics in our inter-component FC analyses revealed a relatively age-invariant graph structure.

To our knowledge, only three other studies used GICA or similar techniques for investigating brain-wide age differences in network topography (Allen et al. 2011; Huang et al. 2015; Vij et al. 2018). In the first such study, Allen et al. (2011) employed IC scaling methods similar to the ones used in our current work. The authors reported declining intra-network FC (affecting every network component) with age, and those age differences in IC spatial properties could not be fully accounted for by age-related volumetric differences in cortical GM. This is similar to our present results: except for a few clusters, age effects on network topography could not be fully accounted for by age differences in regional GM volume, indicating that FC provides information about brain aging beyond what can be explained using cortical thickness/volume alone. In the second study, Huang et al. (2018) collapsed spatial map intensity values across all voxels in a network and computed average intra-network FC metrics for the entire IC. The authors reported negative associations between age and intra-IC FC in 5 RSNs: auditory, ventral default mode, right executive control, sensorimotor, and visual medial. No positive associations between age and spatial map intensity were detected. However, because the authors estimated age relationships for FC measures after collapsing them across all of the IC's voxels, it was not clear which of the IC's spatial regions were responsible for the aggregate age effects and whether any of their networks displayed age-associated restructuring (i.e., some regions positively associated with age, and others negatively associated with age). In the third study, Vij et al. (2018) reported negative associations between RSN volume and age in most functional systems, with sensorimotor (i.e.,

Table 2 Age differences in component topography

	Cluster peak (MNI152 coordinates)	Anatomy	Cluster volume (mm^3)	RSN cluster's relationship to age	Cluster's gray matter relationship to age	Semi-partial correlation between age and cluster, controlling the latter for gray matter volume
Somatomotor 1						
Cluster A	−56, −6, 34	Left precentral gyrus, left postcentral gyrus [BA3, BA4, BA6, BA2]	952	Linear ↓ [$R^2=0.244$]	Linear ↓ [$R^2=0.671$]	n.s.
Cluster B	58, −2, 28	Right precentral gyrus [BA6, BA4]	424	Linear ↓ [$R^2=0.222$]	Linear ↓ [$R^2=0.577$]	$r=-0.415$ [$p<0.001$]
Visual 1						
Cluster C	0, −66, 6	Left lingual gyrus, left intracalcarine cortex, left precuneus cortex [BA30, BA18, BA19, BA23]	1624	Linear ↓ [$R^2=0.293$]	Linear ↓ [$R^2=0.559$]	$r=-0.328$ [$p<0.001$]
Visual 2						
Cluster D	−12, −82, 50	Left lateral occipital cortex [BA19, BA7]	280	Linear ↓ [$R^2=0.182$]	Linear ↓ [$R^2=0.147$]	$r=-0.320$ [$p<0.001$]
Cluster E	−14, −96, 24	Left occipital pole [BA18]	280	Linear ↓ [$R^2=0.189$]	Linear ↓ [$R^2=0.322$]	$r=-0.233$ [$p=0.008$]
Visual 4						
Cluster F	38, −68, −16	Right occipital fusiform gyrus [BA19, BA18, BA37]	2816	Linear ↓ [$R^2=0.340$]	Linear ↓ [$R^2=0.287$]	$r=-.0544$ [$p<0.001$]
Auditory						
Cluster G	−60, −12, 6	Left planum temporale, left Heschl's gyrus [BA41, BA42, BA22]	160	Linear ↓ [$R^2=0.189$]	Linear ↓ [$R^2=0.470$]	$r=-0.233$ [$p=0.010$]
Default mode 1						
Cluster H	54, −52, 36	Right angular gyrus [BA40, BA39]	312	Linear ↑ [$R^2=0.201$]	Linear ↓ [$R^2=0.084$]	$r=0.504$ [$p<0.001$]
Cluster I	56, −54, 12	Right middle temporal gyrus, right angular gyrus [BA39, BA22]	176	Linear ↑ [$R^2=0.211$]	Linear ↓ [$R^2=0.103$]	$r=0.450$ [$p<0.001$]
Default mode 2						
Cluster J	−8, −66, 16	Left supracalcarine cortex, left precuneus cortex, left intracalcarine cortex [BA30, BA18, BA23, BA31]	1328	Nonlinear ↓ [$R^2=0.231$]	Linear ↓ [$R^2=0.436$]	$r=-0.446$ [$p<0.001$]
Default mode 4						
Cluster K	−4, 40, −2	Left anterior cingulate gyrus, right anterior cingulate gyrus, left paracingulate gyrus, right paracingulate gyrus, left frontal pole [BA32, BA24, BA9, BA10]	3392	Linear ↓ [$R^2=0.182$]	Linear ↓ [$R^2=0.513$]	$r=-0.208$ [$p=0.018$]
Cluster L	2, 34, 20	Left anterior cingulate gyrus, right anterior cingulate gyrus, left paracingulate gyrus, right paracingulate gyrus [BA32, BA24]	1400	Linear ↓ [$R^2=0.173$]	Linear ↓ [$R^2=0.646$]	n.s.

Table 2 (continued)

	Cluster peak (MNI152 coordinates)	Anatomy	Cluster volume (mm^3)	RSN cluster's relationship to age	Cluster's gray matter relationship to age	Semi-partial correlation between age and cluster, controlling the latter for gray matter volume
Cluster M	−42, 14, −6	Left insular cortex [BA13]	224	Linear ↓ [$R^2=0.238$]	Linear ↓ [$R^2=0.437$]	$r=-0.420$ [$p<0.001$]
Default mode 6						
Cluster N	−52, −32, 2	Left superior temporal gyrus [BA22, BA21]	1448	Linear ↓ [$R^2=0.253$]	Linear ↓ [$R^2=0.257$]	$r=-0.407$ [$p<0.001$]
Cluster O	52, −32, 2	Right superior temporal gyrus [BA22, BA41]	840	Linear ↓ [$R^2=0.230$]	Linear ↓ [$R^2=0.339$]	$r=-0.341$ [$p<0.001$]
Dorsal attention						
Cluster P	44, −60, 46	Right lateral occipital cortex, right angular gyrus, right supramarginal gyrus [BA39, BA40, BA7, BA19]	1488	Nonlinear ↑ [$R^2=0.278$]	Linear ↓ [$R^2=0.422$]	$r=0.536$ [$p<0.001$]
Cluster Q	−48, −52, 48	Left angular gyrus, left supramarginal gyrus [BA40]	144	Linear ↑ [$R^2=0.207$]	Linear ↓ [$R^2=0.090$]	$r=0.447$ [$p<0.001$]
Cluster R	−8, −72, 60	Left lateral occipital cortex [BA7]	112	Linear ↓ [$R^2=0.193$]	n.s.	$r=-0.451$ [$p<0.001$]
Executive control 2						
Cluster S	38, 58, 14	Right frontal pole [BA10, BA9]	480	Linear ↓ [$R^2=0.169$]	n.s.	$r=-0.408$ [$p<0.001$]
Mixed 3						
Cluster T	52, −58, 8	Right middle temporal gyrus (temporooccipital part), right lateral occipital cortex (inferior division) [BA39, BA37]	352	Linear ↓ [$R^2=0.203$]	Linear ↓ [$R^2=0.181$]	$r=-0.356$ [$p<0.001$]
Cluster U	−50, −54, 12	Left middle temporal gyrus (temporooccipital part), left angular gyrus [BA39]	104	Linear ↓ [$R^2=0.160$]	Nonlinear ↓ [$R^2=0.077$]	$r=-0.354$ [$p<0.001$]
Mixed 4						
Cluster V	−48, 16, −6	Left inferior frontal gyrus (*pars triangularis* and *pars opercularis*), left orbitofrontal cortex, left frontal operculum [BA47, BA44, BA45, BA46, BA22, BA13]	7192	Linear ↓ [$R^2=0.295$]	Linear ↓ [$R^2=0.542$]	$r=-0.280$ [$p<0.001$]
Cluster W	50, 24, −4	Right inferior frontal gyrus (*pars triangularis* and *pars opercularis*), right orbitofrontal cortex, right frontal operculum, right frontal pole [BA45, BA47, BA44, BA46, BA9, BA13]	6464	Linear ↓ [$R^2=0.322$]	Linear ↓ [$R^2=0.483$]	$r=-0.394$ [$p<0.001$]

This table complements Figs. 7, 8, 9, and 10

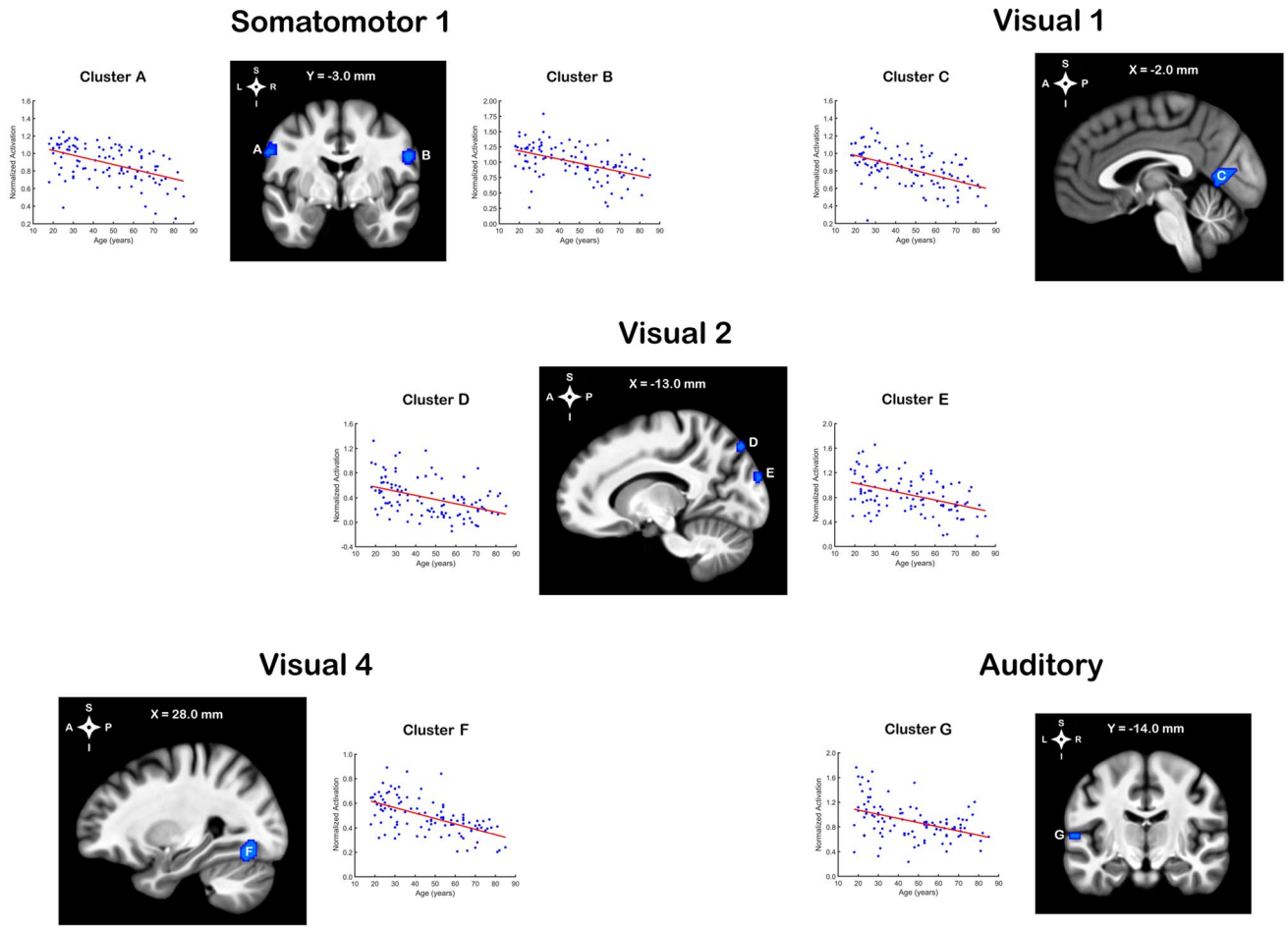

Fig. 7 Clusters with statistical relationships to age for sensorimotor network ICs. Each cluster represents brain region(s) with age differences in network topography. Regression plots represent voxel-averaged fractional polynomial follow-ups. Since spatial maps were normalized by peak activation amplitude, values close to 1 represent network core, while those close to 0 represent network periphery

visual, somatomotor, auditory) networks being especially vulnerable to age-related decline. However, those negative associations between RSN volume and age were not limited to sensorimotor regions: executive, salience, and basal ganglia networks also displayed lower component volumes in aging adults. In addition, 2 network components—posterior default mode and central executive control—showed positive associations with age, indicating that at least in some cognitive regions of the brain, there is a pattern of intra-network reorganization occurring throughout life, as opposed to an outright loss of network structure. Despite these insights, it should be noted that Vij et al. (2018) defined network volume as the number of voxels in a subject's component map above a predefined *z*-statistic cutoff. Consequently, it was not clear whether age differences in RSN volumes were caused by age differences in network structure or age differences in network amplitude.

Rather than *z*-scoring our IC spatial maps, we normalized our IC spatial maps by BOLD amplitude, which more accurately captures true group differences in spatial features (Allen et al. 2011, 2012). We also performed voxel-based age comparisons, enabling us to detect both increases and decreases in intra-component FC. According to our age comparisons of IC topography, the three largest age relationship clusters were localized within the frontal lobes, and all three showed negative linear relationships between the amplitude-normalized SM intensity and age. Two of those clusters belonged to the 'Mixed 4' network component and were located primarily within the bilateral inferior frontal gyrus and bilateral orbitofrontal cortex. The third cluster represented bilateral anterior cingulate and bilateral paracingulate regions of the DMN's frontal subsystem. In addition to frontal lobes, we identified age relationship clusters in the parietal, visual, and temporal regions of the brain. Of these, parietal networks deserve special attention since only the parietal association cortex contained clusters representing both positive and negative correlations to age, indicating age-related network

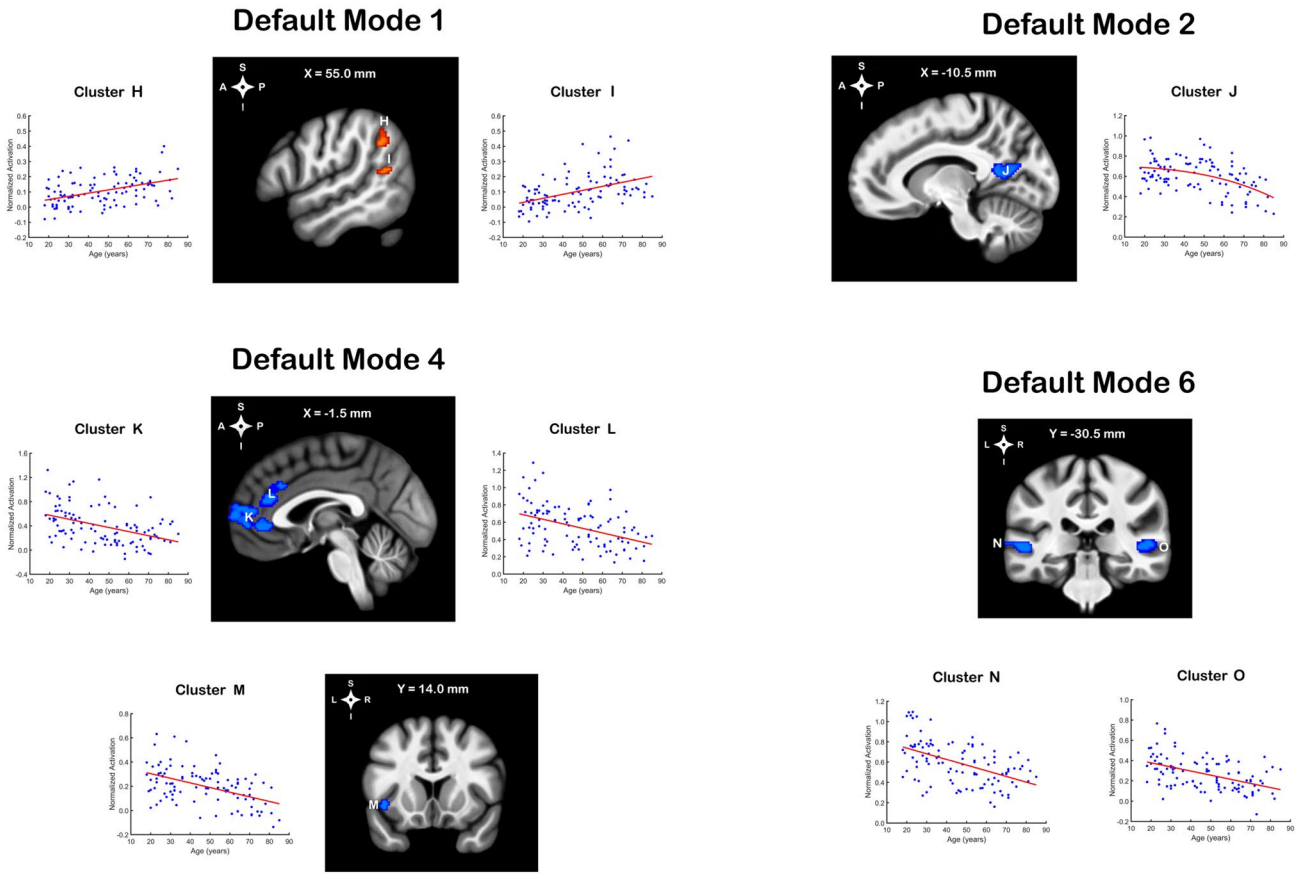

Fig. 8 Clusters with statistical relationships to age for the default mode network components. Blue clusters represent negative association to age; red clusters represent positive association to age

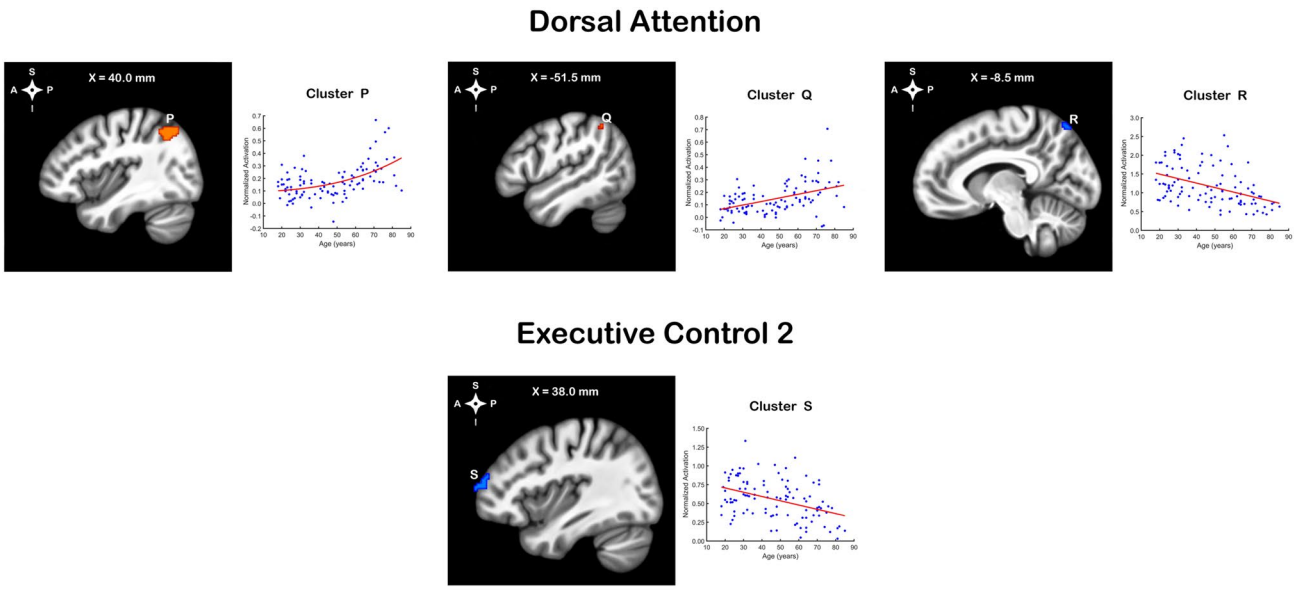

Fig. 9 Clusters with statistical relationships to age for the attention-related network components. Blue clusters represent negative age relationships; red clusters represent positive age relationships

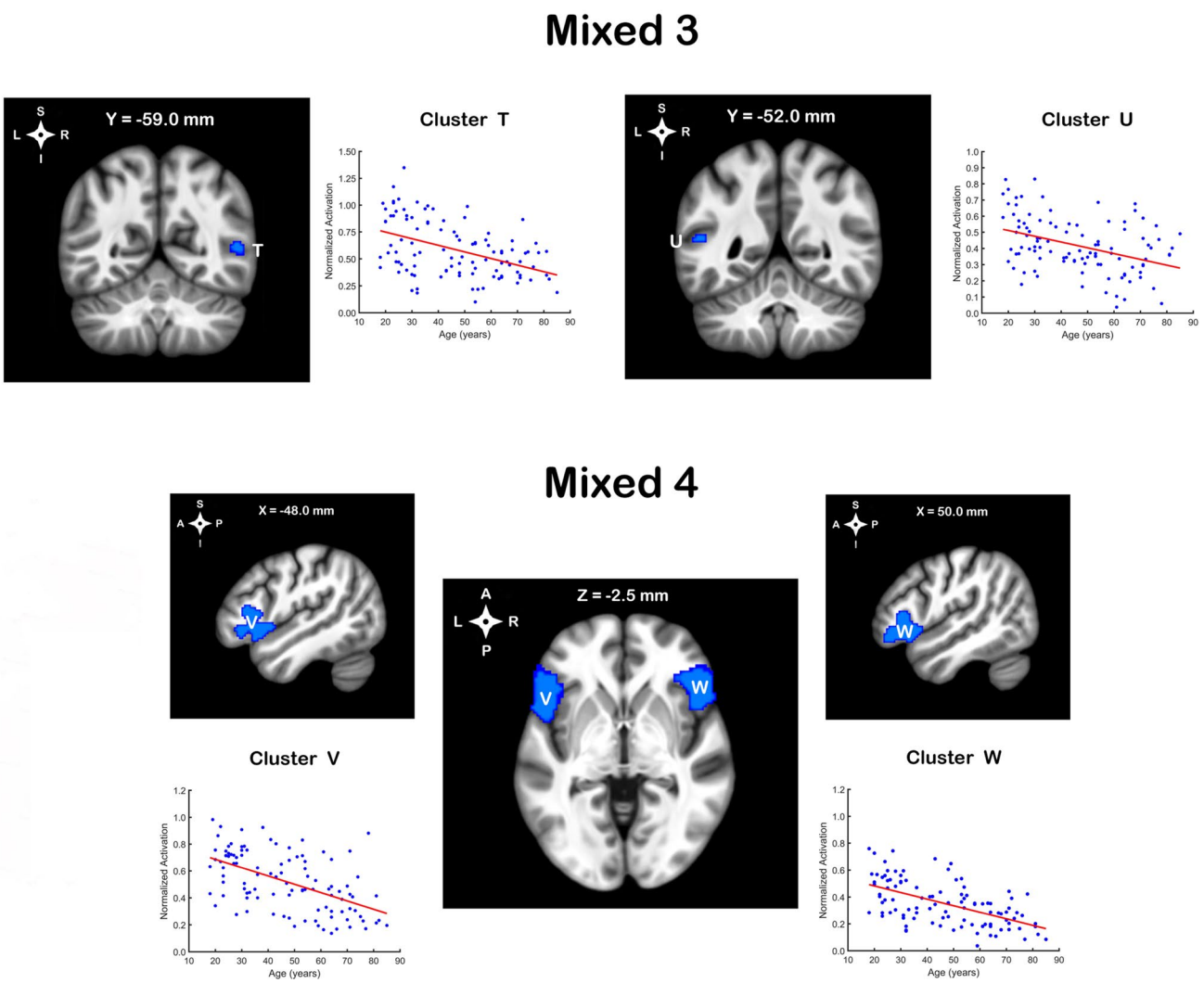

Fig. 10 Clusters with statistical relationships to age for multi-system (i.e., 'Mixed') network components. All statistically significant clusters in 'Mixed' ICs showed negative associations to age

restructuring in those regions. A number of recent studies by other groups, employing different network estimation techniques, also detected complex aging-related network re-wiring in the parietal association cortex (Grady et al. 2016; Meunier et al. 2009; Onoda and Yamaguchi 2013; Park et al. 2010).

Initial imaging evidence for altered network dynamics in old age was demonstrated in task-based fMRI and PET experiments, which showed an over-recruitment of frontal and parietal association cortices in older cohorts in a wide variety of cognitive tasks (Cabeza et al. 2002, 2004; Davis et al. 2008; Grady et al. 1994; Gutchess et al. 2005; Li et al. 2015; Logan et al. 2002; Rypma and D'Esposito 2000; Rajah and D'Esposito 2005; Schneider-Garces et al. 2010; Spreng et al. 2010; Sugiura, 2016). Age effects on network dynamics were reported even in simple motor experiments, during which older adults showed greater activity in the ipsilateral somatomotor cortex, supplementary motor and premotor areas, basal ganglia, as well as association regions in the parietal cortex (Kim et al. 2010; Riecker et al. 2006; Tsvetanov et al. 2015). This additional activity seems to be compensatory in nature and plays a vital role in maintaining cognitive performance in older adults (Fera et al. 2005; Park and Reuter-Lorenz 2009; Rossi et al. 2004; Solé-Padullés et al. 2006; Schneider-Garces et al. 2010).

Recently, interest has grown in graph theory and its ability to summarize age effects on the brain's functional architecture (Rubinov and Sporns 2010; Damoiseaux 2017; Wig 2017). In general, brain-aging studies that employed graphical models to study FC indicate functional dedifferentiation among old adults, typically manifesting as a less distinct or less stable grouping of certain brain areas into network

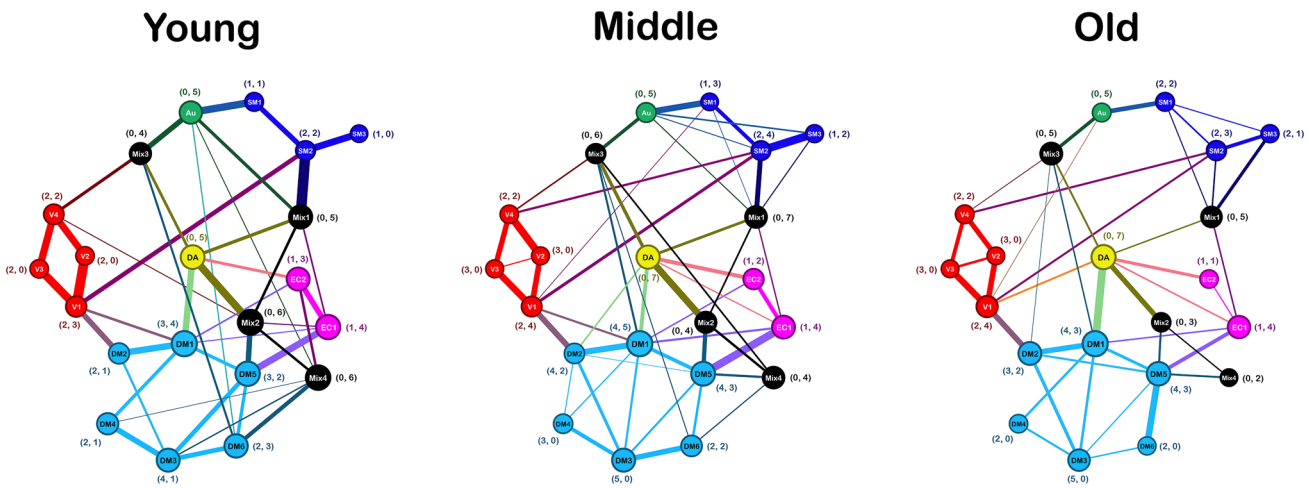

Fig. 11 Graphical representation of direct between-component connectivity separated by age group. Only positive correlations are shown. Edge thickness represents functional connectivity strength (i.e., magnitude of SCAD-regularized partial correlations). Node size of each network component represents its unweighted eigenvector centrality. Coordinates depict the number of within-system (left number) and between-system (right number) connections. Node colors represent functional systems: blue, somatomotor (SM); red, visual (V); green, auditory (Au); cyan, default mode (DM); yellow, dorsal attention (DA); magenta, executive control (EC); black, mixed (Mix). See Fig. 2 for anatomical profiles of individual network components

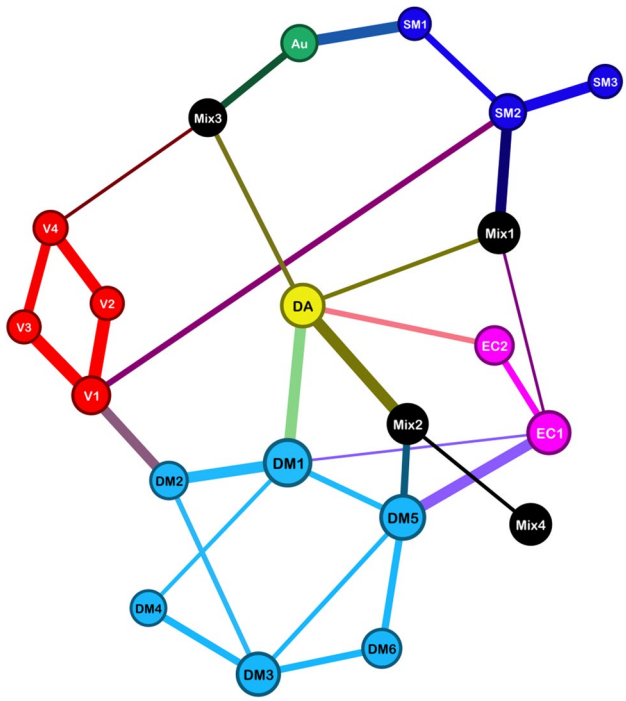

Fig. 12 A core set of inter-component connections that were present in every age group (i.e., young, middle-aged, old). Edge thickness represents connectivity strength, collapsed across age groups. SM, somatomotor (blue); V, visual (red); Au, auditory (green); DM, default mode (cyan); DA, dorsal attention (yellow); EC, executive control (magenta); Mix, mixed (black)

communities (Chan et al. 2014; Chong et al. 2019; Geerligs et al. 2015; Grady et al. 2016; Keller et al. 2015; Onoda and Yamaguchi 2013; Spreng et al. 2016; Vij et al. 2018). However, since almost all previous FC studies that relied on graphical methods estimated their graphs using bivariate, not partial correlations, their results may have been confounded by indirect connections (Epskamp and Fried 2018; Smith et al. 2011). To our best knowledge, this is the first study to combine sparse graphical estimation methods with ICA-based network extraction to investigate age effects on inter-component FC.

Consistent with other graph-based FC studies of brain aging, our weighted efficiency-related graph summary metrics (i.e., global efficiency, characteristic path length, network diameter, and network radius) suggest that functional communication in the human brain becomes increasingly inefficient with age [$\text{Efficiency}_{\text{young}} > \text{Efficiency}_{\text{middle-aged}} > \text{Efficiency}_{\text{old}}$]. Furthermore, as evidenced by weighted closeness and betweenness centralities, age differences were primarily characterized by a widespread reduction in network integration in old relative to young adults—and not by any particular IC's importance to the overall information flow in the human brain. Despite this broad loss of network efficiency in old age, our unweighted graph summary metrics indicate that the fundamental network architecture is stable in young, middle, and late adulthood. We also want to point out that age differences in the overall edge weight were more pronounced in young vs. middle-aged comparisons than in middle-aged vs. old comparisons indicating relatively early aging effects on FC.

Table 3 Global graph summary metrics, separated by age group, for binary and weighted inter-component functional connectivity

	Binarized				Weighted			
	Young	Middle	Old	Statistical differences	Young	Middle	Old	Statistical differences
Density	0.2095	0.2476	0.2095	None	0.0443	0.0419	0.0328	Young > Old*** Middle > Old***
Efficiency	0.5413	0.5698	0.5290	None	0.1145	0.0975	0.0840	Young > Old*** Young > Middle*** Middle > Old*
Transitivity	0.2195	0.3974	0.3373	None	0.0365	0.0611	0.0489	None
Radius	3	2	3	None	12.7969	16.0334	18.3483	Young < Old** Young < Middle*
Diameter	4	4	4	None	21.5832	25.7084	32.4533	Young < Old*** Young < Middle* Middle < Old*
Characteristic path length	2.0862	1.9864	2.1859	None	10.5684	12.3702	14.3148	Young < Old*** Young < Middle** Middle < Old*
Average edge weight	N/A	N/A	N/A	N/A	0.2117	0.1692	0.1565	Young > Old** Young > Middle*
Intra-system edge density	0.6000	0.7600	0.7600	Young < Old** Young < Middle*	0.1589	0.1522	0.1318	Young > Old** Middle > Old*
Inter-system edge density	0.1568	0.1784	0.1351	None	0.0289	0.0270	0.0194	Young > Old** Middle > Old**
Average weight of intra-system connections	N/A	N/A	N/A	N/A	0.2648	0.2003	0.1734	Young > Old*** Young > Middle**
Average weight of inter-system connections	N/A	N/A	N/A	N/A	0.1842	0.1513	0.1436	None
Degree centralization	0.1553	0.2237	0.1553	None	N/A	N/A	N/A	N/A
Closeness centralization	0.1673	0.2977	0.3070	Young < Old ˜ Young < Middle ˜	N/A	N/A	N/A	N/A
Betweenness centralization	0.1249	0.1424	0.1566	None	N/A	N/A	N/A	N/A

***FDR < 0.001; **FDR < 0.010; *FDR < .050; ˜ FDR < 0.100

In general, intra-system FC strength was more vulnerable to aging than inter-system FC strength; however, certain inter-system connections, especially those connected to the 'Mixed' ICs, showed age-associated FC decline that was evident by middle adulthood.

Contrary to some previous research (e.g., Betzel et al. 2014; Chan et al. 2014; Geerligs et al. 2015; Spreng et al. 2016), we did not find substantial evidence for greater inter-system integration in old age: almost all edges with age differences in our FDR-corrected age comparisons represented connections between one of the clearly defined RSNs and one of the 'Mixed' (i.e., multi-system) RSNs. Since those 'Mixed' RSNs act as hubs that interconnect multiple functional systems with each other, declining FC between these multi-system RSNs and other systems is also indicative of less efficient network architecture. Of particular note here is the loss of connectivity between the DM6 and Mix4 components with age. Structurally, the Mix4 IC showed the largest topographical age differences, especially in the bilateral inferior frontal gyrus. As these regions become increasingly disconnected from the rest of the component with age, the entire IC loses its connectivity to the DM6 IC. With a less strict statistical threshold (uncorrected $p < 0.010$), we identified additional age differences in inter-component FC, primarily among various default mode sub-systems (Andrews-Hanna et al. 2014; Christoff et al. 2016). Early FC experiments showed that communication between distant areas of the DMN, especially between the medial frontal and posterior cingulate/retrosplenial hubs, declines with age (Andrews-Hanna et al. 2007; Damoiseaux et al. 2008; Wu et al. 2011). More recent work, employing not only cross-sectional but also longitudinal designs, produced mixed results with some groups supporting the early findings (e.g., Geerligs et al. 2015; Grady et al. 2016; Ng et al. 2016) and others finding no age effects (Hirsiger et al. 2016; Persson et al. 2014). Our inter-component FC results demonstrated a relatively complex pattern of age-related network reorganization within this system. Age-related shifts in the DMN's organization could represent age differences in spontaneous thought processes or changes in network architecture away

Table 4 Age differences in node centrality for weighted inter-component functional connectivity graphs

RSN	Degree		Closeness		Betweenness		Eigenvector	
	Young/middle/old	Statistical differences	Young/middle/old	Statistical differences	Young/middle/old	Statistical differences	Young/middle/old	Statistical differences
SM1	0.584/0.633/0.514	None	1.752/1.415/1.086	**Y > O, *Y > M	0.042/0.021/0.026	None	0.115/0.113/0.056	None
SM2	1.248/1.196/0.667	**Y > O, *M > O	2.153/1.784/1.364	**Y > O, *Y > M	0.216/0.190/0.084	None	0.252/0.194/0.110	*Y > O
SM3	0.317/0.566/0.454	None	1.647/1.483/1.213	**Y > O	0.000/0.000/0.000	None	0.082/0.107/0.055	None
Vis1	1.429/1.227/1.155	**Y > O	2.135/1.912/1.796	*Y > O, *Y > M	0.205/0.258/0.305	None	0.311/0.273/0.336	None
Vis2	0.754/0.709/0.665	None	1.839/1.542/1.434	**Y > O, *Y > M	0.047/0.037/0.063	None	0.196/0.146/0.189	None
Vis3	0.701/0.662/0.652	None	1.802/1.566/1.457	**Y > O, *Y > M	0.000/0.000/0.000	None	0.177/0.144/0.193	None
Vis4	0.911/0.847/0.663	None	1.748/1.545/1.314	*Y > O	0.058/0.032/0.011	None	0.172/0.142/0.141	None
Au	0.940/0.749/0.475	**Y > O	1.808/1.444/1.198	**Y > O, *Y > M	0.053/0.042/0.047	None	0.147/0.115/0.083	None
DM1	1.307/1.390/1.267	None	2.251/2.069/1.971	*Y > O	0.163/0.195/0.195	None	0.300/0.372/0.461	**Y < O
DM2	0.693/0.993/0.894	*Y < M	2.154/2.026/1.857	*Y > O	0.037/0.232/0.190	None	0.198/0.298/0.370	**Y < O, *Y < M
DM3	0.956/0.876/0.649	None	1.852/1.614/1.444	*Y > O	0.037/0.068/0.000	None	0.165/0.205/0.238	None
DM4	0.514/0.385/0.265	None	1.617/1.221/1.224	*Y > O, *Y > M	0.005/0.000/0.000	None	0.110/0.111/0.115	None
DM5	1.143/1.228/1.130	None	2.025/1.755/1.586	*Y > O	0.079/0.084/0.195	None	0.255/0.305/0.321	None
DM6	0.837/0.580/0.409	*Y > O	1.771/1.490/1.301	**Y > O	0.058/0.011/0.000	None	0.145/0.130/0.150	None
DA	1.129/1.238/1.214	None	2.340/1.961/1.967	*Y > O, *Y > M	0.158/0.116/0.237	None	0.278/0.306/0.390	*Y < O
EC1	0.875/0.885/0.611	None	1.793/1.609/1.400	*Y > O	0.011/0.047/0.042	None	0.209/0.253/0.215	None
EC2	0.686/0.513/0.262	**Y > O	1.657/1.483/1.302	*Y > O	0.016/0.016/0.000	None	0.158/0.164/0.105	None
Mix1	1.076/0.864/0.579	**Y > O	2.230/1.720/1.361	**Y > O, *Y > M	0.153/0.084/0.068	None	0.262/0.184/0.109	*Y > O
Mix2	1.071/0.779/0.471	**Y > O	2.188/1.725/1.542	**Y > O, *Y > M	0.105/0.032/0.026	None	0.261/0.210/0.175	None
Mix3	0.705/0.793/0.550	None	2.000/1.807/1.379	**Y > O	0.079/0.126/0.090	None	0.132/0.173/0.178	None
Mix4	0.752/0.488/0.221	**Y > O	1.556/1.389/1.039	**Y > O	0.005/0.000/0.000	None	0.132/0.111/0.069	None

Abbreviations: SM, somatomotor; Vis, visual; Au, auditory; DM, default mode; DA, dorsal attention; EC, executive control; Mix, mixed
**FDR < 0.010; *FDR < 0.050

from long-range communication to favor anatomically proximal short-range communication (as suggested by Tomasi and Volkow 2012). Even though our data suggest age differences in the architecture of the default mode system, these findings should be interpreted with caution since they did not survive the FDR correction for multiple hypothesis testing.

Limitations

In light of our results on network amplitude, caution should be exercised when interpreting FC measures without additional knowledge of how non-BOLD contribution to the fMRI time series is affected in healthy aging. For similar reasons, findings from other studies on functional dedifferentiation with age should also be interpreted with caution, since age effects on BOLD amplitude (and consequently temporal SNR) might be responsible for lower correlation strength in old adults, which in turn would result in less stable estimates of network community structure. Due to technical and computational limitations, we relied on linear and quadratic regression models in our initial screening for age differences in components' topography. We do not consider this to be a major issue in our study as most linear, curved, and u-shaped patterns can be detected using quadratic and linear fits. To further mitigate the downsides of linear and quadratic fits (Aghamohammadi-Sereshki et al. 2019; Fjell et al. 2010), all clusters showing statistical age

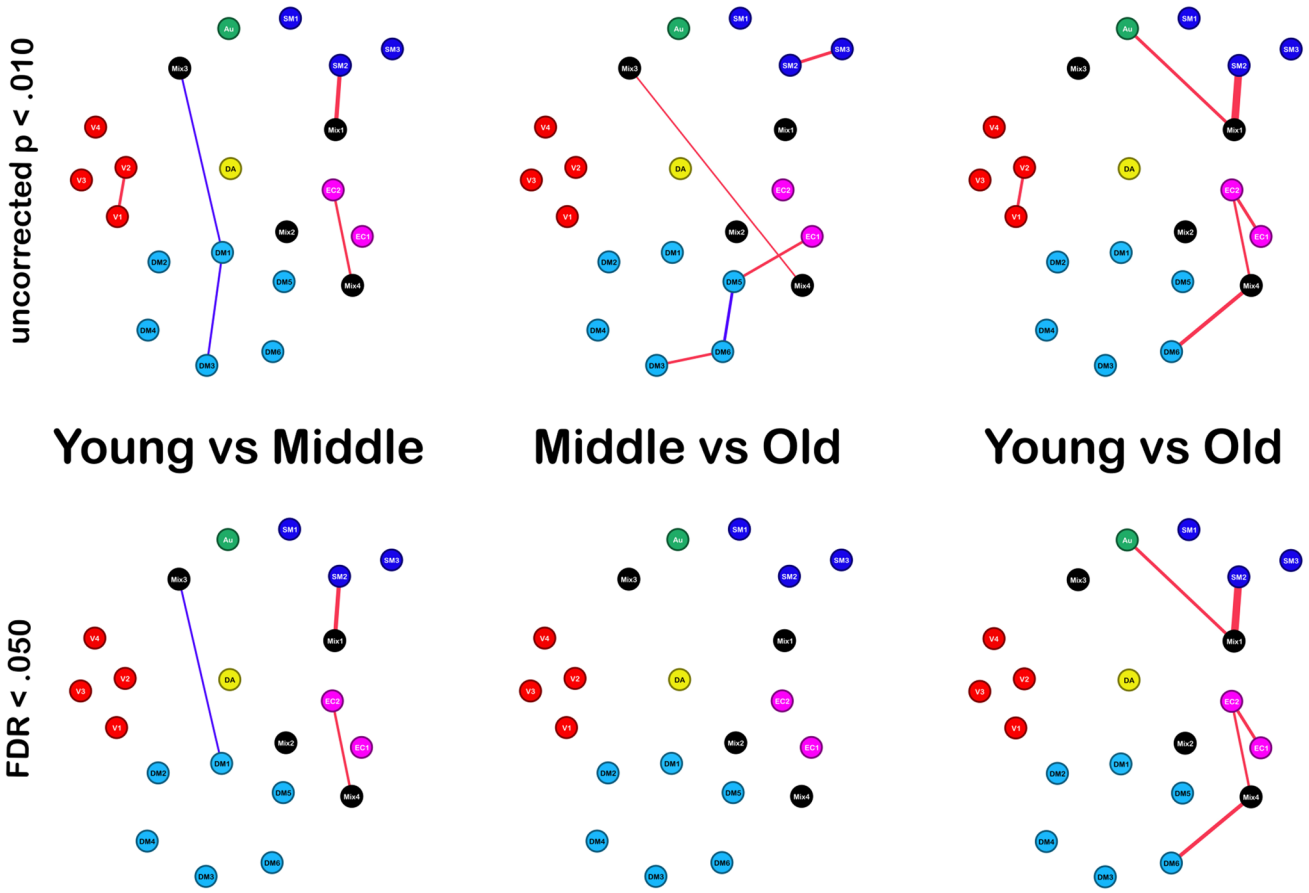

Fig. 13 Graphical representations of uncorrected (top) and FDR-corrected (bottom) age differences in inter-component functional connectivity. Red edge color represents lower functional connectivity in the older group; blue edge color represents greater functional connectivity in the older group. Edge thickness represents the magnitude of functional connectivity differences in each age comparison. Nodes represent network components: SM, somatomotor; V, visual; Au, auditory; DM, default mode; DA, dorsal attention; EC, executive control; Mix, mixed. See Fig. 2 for anatomical profiles of each node/RSN

differences were followed up with fractional polynomial modeling.

It is important to keep in mind that head motion has been shown to modulate FC in multiple RSNs (Mowinckel et al. 2012; Power et al. 2012; Van Dijk et al. 2012). As is typically reported in the field (e.g., Madan 2018), our older participants were not as still inside the scanner as younger ones (see Suppl. Table 3). Motion correction methods based on spatial ICA provide a balanced approach for artefact removal (Ciric et al. 2017; Griffanti et al. 2014; Pruim et al. 2015b). To further ensure thorough removal of dominant physiological and motion artifacts, we performed aggressive, as opposed to soft, removal of global noise components and used partial, as opposed to full, correlations for studying inter-component FC. Since we employed fairly rigorous denoising procedures, we believe that our findings represent non-artefactual age differences in network properties. This is further supported by our young vs. middle-aged comparisons of network amplitude and inter-component FC: both sets of analyses showed substantial age differences even though head motion parameters did not differ between the two age groups (see Suppl. Table 3). Nonetheless, acquisitions that employ customized physical restrains (Power et al. 2019) and direct measures of physiological noise (Birn et al. 2006, 2008; Chang et al. 2009; Glover et al. 2000) are needed to confirm the neurobiological origin of our findings.

Furthermore, it is plausible that negative connections might contain additional information about the effects of age on FC. However, incorporating anti-correlations into our inter-component graph-based comparisons would have produced summary metrics that are difficult to interpret (Rubinov and Sporns 2010), while separate age comparisons of negative edges do not integrate anti-correlations into the broader connectome. Consequently, we did not study the effects of age on negative connections. As a reference for future research, we provide descriptive visuals of

Table 5 Age differences in edge connectivity strength for weighted inter-component functional connectivity graphs

	Young (*r*)	Middle (*r*)	Old (*r*)	Young vs. middle (uncorrected *p*)	Middle vs. old (uncorrected *p*)	Young vs. old (uncorrected *p*)	FDR-corrected age differences
SM2 ↔ Mix1	0.460	0.243	0.107	$p < 0.001$	n.s.	$p < 0.001$	Young > old Young > middle
EC2 ↔ Mix4	0.147	0.000	0.000	$p < 0.002$	n.s.	$p < 0.001$	Young > old Young > middle
EC1 ↔ EC2	0.270	0.211	0.094	n.s.	$p < 0.040$	$p < 0.003$	Young > old
Au ↔ Mix1	0.173	0.088	0.000	n.s.	n.s.	$p < 0.003$	Young > old
DM6 ↔ Mix4	0.205	0.094	0.000	n.s.	n.s.	$p < 0.005$	Young > old
DM1 ↔ Mix3	0.000	0.127	0.103	$p < 0.002$	n.s.	$p < 0.040$	Young < middle
Vis1 ↔ Vis2	0.433	0.271	0.271	$p \approx 0.010$	n.s.	$p < 0.007$	None
DM1 ↔ DM3	0.000	0.131	0.150	$p < 0.006$	n.s.	$p < 0.020$	None
DM5 ↔ EC1	0.311	0.349	0.192	n.s.	$p < 0.002$	$p < 0.020$	None
DM3 ↔ DM6	0.233	0.257	0.103	n.s.	$p < 0.003$	$p < 0.030$	None
DM5 ↔ DM6	0.174	0.144	0.306	n.s.	$p < 0.005$	$p < 0.020$	None
SM2 ↔ SM3	0.317	0.366	0.192	n.s.	$p < 0.009$	n.s.	None
Mix3 ↔ Mix4	0.000	0.115	0.000	$p < 0.020$	$p < 0.010$	n.s.	None

Only edges that survived the uncorrected $p < 0.01$ threshold in at least one age comparison are shown

Abbreviations: SM, somatomotor; Vis, visual; Au, auditory; DM, default mode; DA, dorsal attention; EC, executive control; Mix, mixed. This table accompanies Fig. 13

SCAD-estimated negative connections in the Supplementary Materials (Suppl. Figure 10).

We also need to emphasize that our study was cross-sectional, and a longitudinal sample is needed to confirm our results as real aging, not cohort, effects. Lastly, future research would benefit from addressing the issue of sex differences in brain aging. Even though we did not attain sufficient statistical power to perform sex comparisons in our inter-component FC graphs (< 15 males in middle-aged and old adult groups), we were able to test for male vs. female differences in network topography and BOLD amplitude. Those analyses did not reveal any statistically significant sex effects or interactions. However, in those analyses, too, potential consequences of limited statistical power come to mind: it is plausible that sex differences in brain aging are subtle, and a larger sample is necessary to detect them.

Supplementary Information The online version contains supplementary material available at https://doi.org/10.1007/s00429-021-02226-7.

Acknowledgements This project was supported by the Canadian Institutes of Health Research (CIHR) operating grant (MOP11501) and the Natural Sciences and Engineering Research Council of Canada (NSERC) operating grant (06186) to N.V.M. S.H. was supported by the CIHR Doctoral Scholarship. The work of I.C. was partially supported by the NSERC operating grant (06638) and the Xerox Faculty Fellowship, Alberta School of Business.

Author contributions Conceptualization: SH and NVM; data collection: FO, PS, RC and NVM; data analysis: SH, IC, JM, CRM and NVM; manuscript writing, SH and NVM. All the co-authors reviewed and approved the final version of the manuscript.

Data availability For confidentiality reasons, imaging data are not publicly available.

Code availability Most of the analyses were conducted using freely available imaging software. We are willing to share some of our in-house analysis scripts upon request.

Compliance with ethical standards

Conflict of interest All the authors have no conflicts of interest to disclose.

References

Aanerud J, Borghammer P, Chakravarty MM, Vang K, Rodell AB, Jónsdottir KY, Møller A, Ashkanian M, Vafaee MS, Iversen P, Johannsen P, Gjedde A (2012) Brain energy metabolism and blood flow differences in healthy aging. J Cereb Blood Flow Metab 32:1177–1187

Aghamohammadi-Sereshki A, Hrybouski S, Travis S, Huang Y, Olsen F, Carter R, Camicioli R, Malykhin NV (2019) Amygdala subnuclei and healthy cognitive aging. Hum Brain Mapp 40:34–52

Allen EA, Erhardt EB, Eichele T, Mayer AR, Calhoun VD (2010) "Comparison of pre-normalization methods on the accuracy of group ICA results", in *16th Annual Meeting of the Organization for Human Brain Mapping*, 6–10 June, Barcelona, Spain

Allen EA, Erhardt EB, Damaraju E, Gruner W, Segall JM, Silva RF, Havlicek M, Rachakonda S, Fries J, Kalyanam R, Michael AM, Caprihan A, Turner JA, Eichele T, Adelsheim S, Bryan AD,

Bustillo J, Clark VP, Feldstein Ewing SW, Filbey F, Ford CC, Hutchison K, Jung RE, Kiehl KA, Kodituwakku P, Komesu YM, Mayer AR, Pearlson GD, Phillips JP, Sadek JR, Stevens M, Teuscher U, Thoma RJ, Calhoun VD (2011) A baseline for the multivariate comparison of resting-state networks. Front Syst Neurosci 5:2

Allen EA, Erhardt EB, Wei Y, Eichele T, Calhoun VD (2012) Capturing inter- subject variability with group independent component analysis of fMRI data: a simulation study. NeuroImage 59:4141–4159

Ambler G, Royston P (2001) Fractional polynomial model selection procedures: investigation of type I error rate. J Stat Comput Simul 69:89–108

Ances BM, Liang CL, Leontiev O, Perthen JE, Fleisher AS, Lansing AE, Buxton RB (2009) Effects of aging on cerebral blood flow, oxygen metabolism, and blood oxygenation level dependent responses to visual stimulation. Hum Brain Mapp 30:1120–1132

Andersson JL, Hutton C, Ashburner J, Turner R, Friston K (2001) Modeling geometric deformations in EPI time series. NeuroImage 13:903–919

Andrews-Hanna JR (2012) The brain's default network and its adaptive role in internal mentation. Neuroscientist 18:251–270

Andrews-Hanna JR, Snyder AZ, Vincent JL, Lustig C, Head D, Raichle ME, Buckner RL (2007) Disruption of large-scale brain systems in advanced aging. Neuron 56:924–935

Arbabshirani MR, Damaraju E, Phlypo R, Plis S, Allen E, Ma S, Mathalon D, Preda A, Vaidya JG, Adali T, Calhoun VD (2014) Impact of autocorrelation on functional connectivity. NeuroImage 102(Pt 2):294–308

Avants B, Gee JC (2004) Geodesic estimation for large deformation anatomical shape averaging and interpolation. NeuroImage 23(Suppl 1):S139–S150

Avants BB, Epstein CL, Grossman M, Gee JC (2008) Symmetric diffeomorphic image registration with cross-correlation: evaluating automated labeling of elderly and neurodegenerative brain. Med Image Anal 12:26–41

Bastian M, Heymann S, Jacomy M (2009) Gephi: an open source software for exploring and manipulating networks. In: Third International AAAI Conference on Weblogs and Social Media, pp. 361e362. http://aaai.org/ocs/index.php/ICWSM/09/paper/view/154

Beason-Held LL, Kraut MA, Resnick SM (2008) I. Longitudinal changes in aging brain function. Neurobiol Aging 29:483–496

Beckmann CF, Smith SM (2004) Probabilistic independent component analysis for functional magnetic resonance imaging. IEEE Trans Med Imaging 23:137–152

Bell AJ, Sejnowski T (1995) An information-maximization approach to blind separation and blind deconvolution. Neural Comput 7:1129–1159

Bertsch K, Hagemann D, Hermes M, Walter C, Khan R, Naumann E (2009) Resting cerebral blood flow, attention, and aging. Brain Res 1267:77–88

Betzel RF, Byrge L, He Y, Goñi J, Zuo X-N, Sporns O (2014) Changes in structural and functional connectivity among resting-state networks across the human lifespan. NeuroImage 102(Pt 2):345–357

Biagi L, Abbruzzese A, Bianchi MC, Alsop DC, Del Guerra A, Tosetti M (2007) Age dependence of cerebral perfusion assessed by magnetic resonance continuous arterial spin labeling. J Magn Reson Imaging 25(4):696–702

Birkes D, Dodge Y (1993) Alternative methods of regression. John Wiley & Sons Inc, Hoboken

Birn RM, Diamond JB, Smith MA, Bandettini PA (2006) Separating respiratory-variation-related fluctuations from neuronal-activity-related fluctuations in fMRI. NeuroImage 31(4):1536–1548

Birn RM, Murphy K, Bandettini PA (2008) The effect of respiration variations on independent component analysis results of resting state functional connectivity. Hum Brain Mapp 29(7):740–750

Brown TA, Di Nardo PA, Lehman CL, Campbell LA (2001) Reliability of DSM-IV anxiety and mood disorders: implications for the classification of emotional disorders. J Abnorm Psychol 110:49–58

Buckner RL (2004) Memory and executive function in aging and AD: multiple factors that cause decline and reserve factors that compensate. Neuron 44:195–208

Buckner RL, Snyder AZ, Sanders AL, Raichle ME, Morris JC (2000) Functional brain imaging of young, nondemented, and demented older adults. J Cogn Neurosci 12(Suppl 2):24–34

Buckner RL, Krienen FM, Yeo BTT (2013) Opportunities and limitations of intrinsic functional connectivity MRI. Nat Neurosci 16:832–837

Bullmore E, Sporns O (2009) Complex brain networks: graph theoretical analysis of structural and functional systems. Nat Rev Neurosci 10:186–198

Burnham KP, Anderson DR (2002) Model selection and multimodel inference: a practical information-theoretic approach, 2nd edn. Springer-Verlag, New York

Cabeza R, Anderson ND, Locantore JK, McIntosh AR (2002) Aging gracefully: compensatory brain activity in high-performing older adults. NeuroImage 17:1394–1402

Cabeza R, Daselaar SM, Dolcos F, Prince SE, Budde M, Nyberg L (2004) Task- independent and task-specific age effects on brain activity during working memory, visual attention and episodic retrieval. Cereb Cortex 14:364–375

Calhoun VD, Adali T, Pearlson GD, Pekar JJ (2001) A method for making group inferences from functional MRI data using independent component analysis. Hum Brain Mapp 14:140–151

Cao M, Wang J-H, Dai Z-J, Cao X-Y, Jiang L-L, Fan F-M, Song X-W, Xia M-R, Shu N, Dong Q, Milham MP, Castellanos FX, Zuo X-N, He Y (2014) Topological organization of the human brain functional connectome across the lifespan. Dev Cogn Neurosci 7:76–93

Chan MY, Park DC, Savalia NK, Petersen SE, Wig GS (2014) Decreased segregation of brain systems across the healthy adult lifespan. Proc Natl Acad Sci USA 111:E4997–E5006

Chan MY, Alhazmi FH, Park DC, Savalia NK, Wig GS (2017) Resting-state network topology differentiates task signals across the adult life span. J Neurosci 37:2734–2745

Chang C, Cunningham JP, Glover GH (2009) Influence of heart rate on the BOLD signal: the cardiac response function. NeuroImage 44(3):857–869

Chen JJ, Rosas HD, Salat DH (2011) Age-associated reductions in cerebral blood flow are independent from regional atrophy. NeuroImage 55:468–478

Chong JSX, Ng KK, Tandi J, Wang C, Poh J-H, Lo JC, Chee MWL, Zhou JH (2019) Longitudinal changes in the cerebral cortex functional organization of healthy elderly. J Neurosci 39:5534–5550

Christoff K, Irving ZC, Fox KCR, Spreng RN, Andrews-Hanna JR (2016) Mind- wandering as spontaneous thought: a dynamic framework. Nat Rev Neurosci 17:718–731

Ciric R, Wolf DH, Power JD, Roalf DR, Baum GL, Ruparel K, Shinohara RT, Elliott MA, Eickhoff SB, Davatzikos C, Gur RC, Gur RE, Bassett DS, Satterthwaite TD (2017) Benchmarking of participant-level confound regression strategies for the control of motion artifact in studies of functional connectivity. NeuroImage 154:174–187

Cohen ER, Rostrup E, Sidaros K, Lund TE, Paulson OB, Ugurbil K, Kim S-G (2004) Hypercapnic normalization of BOLD fMRI: comparison across field strengths and pulse sequences. NeuroImage 23:613–624

Costantini G, Epskamp S, Borsboom D, Perugini M, Mõttus R, Waldorp LJ, Cramer AOJ (2015) State of the aRt personality research: A tutorial on network analysis of personality data in R. J Res Pers 54:13–29

Craddock RC, Jbabdi S, Yan C-G, Vogelstein JT, Castellanos FX, Di Martino A, Kelly C, Heberlein K, Colcombe S, Milham MP (2013) Imaging human connectomes at the macroscale. Nat Methods 10:524–539

Crossley NA, Mechelli A, Vértes PE, Winton-Brown TT, Patel AX, Ginestet CE, McGuire P, Bullmore ET (2013) Cognitive relevance of the community structure of the human brain functional coactivation network. Proc Natl Acad Sci USA 110:11583–11588

D'Esposito M, Zarahn E, Aguirre GK, Rypma B (1999) The effect of normal aging on the coupling of neural activity to the bold hemodynamic response. NeuroImage 10:6–14

D'Esposito M, Deouell LY, Gazzaley A (2003) Alterations in the BOLD fMRI signal with ageing and disease: a challenge for neuroimaging. Nat Rev Neurosci 4:863–872

Damoiseaux JS (2017) Effects of aging on functional and structural brain connectivity. NeuroImage 160:32–40

Damoiseaux JS, Beckmann CF, Arigita EJS, Barkhof F, Scheltens P, Stam CJ, Smith SM, Rombouts SARB (2008) Reduced resting-state brain activity in the "default network" in normal aging. Cereb Cortex 18:1856–1864

Davis SW, Dennis NA, Daselaar SM, Fleck MS, Cabeza R (2008) Que PASA? The posterior-anterior shift in aging. Cereb Cortex 18:1201–1209

Deco G, Corbetta M (2011) The dynamical balance of the brain at rest. Neuroscientist 17:107–123

Di Nardo PA, Brown TA, Barlow DH (1994) Anxiety Disorders interview schedule for DSM-IV—Lifetime Version (ADIS-IV-L). Psychological Corporation, San Antonio

Dielman TE (2005) Least absolute value regression: recent contributions. J Stat Comput Simul 75:263–286

Drton M, Perlman MD (2004) Model selection for Gaussian concentration graphs. Biometrika 91:591–602

Du Y, Fan Y (2013) Group information guided ICA for fMRI data analysis. NeuroImage 69:157–197

Du Y, Allen EA, He H, Sui J, Wu L, Calhoun VD (2016) Artifact removal in the context of group ICA: a comparison of single-subject and group approaches. Hum Brain Mapp 37:1005–1025

Du Y, Lin D, Yu Q, Sui J, Chen J, Rachakonda S, Adali T, Calhoun VD (2017) Comparison of IVA and GIG-ICA in brain functional network estimation using fMRI data. Front Neurosci 11:267

Duff EP, Makin T, Cottaar M, Smith SM, Woolrich MW (2018) Disambiguating brain functional connectivity. NeuroImage 173:540–550

Epskamp S, Fried EI (2018) A tutorial on regularized partial correlation networks. Psychol Methods 23:617–634

Fabiani M (2012) It was the best of times, it was the worst of times: a psychophysiologist's view of cognitive aging. Psychophysiology 49:283–304

Fabiani M, Gordon BA, Maclin EL, Pearson MA, Brumback-Peltz CR, Low KA, McAuley E, Sutton BP, Kramer AF, Gratton G (2014) Neurovascular coupling in normal aging: a combined optical, ERP and fMRI study. NeuroImage 85(Pt 1):592–607

Fan J, Li R (2001) Variable selection via nonconcave penalized likelihood and its oracle properties. J Am Stat Assoc 96:1348–1360

Farkas E, Luiten PGM (2001) Cerebral microvascular pathology in aging and Alzheimer's disease. Prog Neurobiol 64:575–611

Fera F, Weickert TW, Goldberg TE, Tessitore A, Hariri A, Das S, Lee S, Zoltick B, Meeter M, Myers CE, Gluck MA, Weinberger DR, Mattay VS (2005) Neural mechanisms underlying probabilistic category learning in normal aging. J Neurosci 25:11340–11348

Fjell AM, Walhovd KB, Fennema-Notestine C, McEvoy LK, Hagler DJ, Holland D, Brewer JB, Dale AM (2009a) One-year brain atrophy evident in healthy aging. J Neurosci 29:15223–15231

Fjell AM, Westlye LT, Amlien I, Espeseth T, Reinvang I, Raz N, Agartz I, Salat DH, Greve DN, Fischl B, Dale AM, Walhovd KB (2009b) High consistency of regional cortical thinning in aging across multiple samples. Cereb Cortex 19:2001–2012

Fjell AM, Walhovd KB, Westlye LT, Østby Y, Tamnes CK, Jernigan TL, Tamnes CK, Jernigan TL, Gamst A, Dale AM (2010) When does brain aging accelerate? Dangers of quadratic fits in cross-sectional studies. NeuroImage 50(4):1376–1383

Fjell AM, Sneve MH, Grydeland H, Storsve AB, de Lange A-MG, Amlien IK, Røgeberg OJ, Walhovd KB (2015) Functional connectivity change across multiple cortical networks relates to episodic memory changes in aging. Neurobiol Aging 36:3255–3268

Frackowiak RS, Lenzi GL, Jones T, Heather JD (1980) Quantitative measurement of regional cerebral blood flow and oxygen metabolism in man using 15O and positron emission tomography: theory, procedure, and normal values. J Comput Assist Tomogr 4(6):727–736

Freedman D, Lane D (1983) A nonstochastic interpretation of reported significance levels. J Business Econ Statistics 1:292

Friedman J, Hastie T, Tibshirani R (2008) Sparse inverse covariance estimation with the graphical lasso. Biostatistics 9:432–441

Gagnon L, Sakadžic S, Lesage F, Musacchia JJ, Lefebvre J, Fang Q, Yücel MA, Evans KC, Mandeville ET, Cohen-Adad J, Polimeni JR, Yaseen MA, Lo EH, Greve DN, Buxton RB, Dale AM, Devor A, Boas DA (2015) Quantifying the microvascular origin of BOLD-fMRI from first principles with two-photon microscopy and an oxygen-sensitive nanoprobe. J Neurosci 35:3663–3675

Galiano A, Mengual E, García de Eulate R, Galdeano I, Vidorreta M, Recio M, Riverol M, Zubieta JL, Fernández-Seara MA (2019) Coupling of cerebral blood flow and functional connectivity is decreased in healthy aging. Brain Imaging Behav. https://doi.org/10.1007/s11682-019-00157-w

Galvin JE, Roe CM, Coats MA, Morris JC (2007) Patient's rating of cognitive ability: using the AD8, a brief informant interview, as a self-rating tool to detect dementia. Arch Neurol 64:725–730

Geerligs L, Renken RJ, Saliasi E, Maurits NM, Lorist MM (2015) A brain-wide study of age-related changes in functional connectivity. Cereb Cortex 25:1987–1999

Glover GH, Li TQ, Ress D (2000) Image-based method for retrospective correction of physiological motion effects in fMRI: RETROICOR. Magn Reson Med 44(1):162–167

Good CD, Johnsrude IS, Ashburner J, Henson RN, Friston KJ, Frackowiak RS (2001) A voxel-based morphometric study of ageing in 465 normal adult human brains. NeuroImage 14(Pt 1):21–36

Gordon EM, Laumann TO, Adeyemo B, Petersen SE (2017) Individual variability of the system-level organization of the human brain. Cereb Cortex 27:386–399

Grady CL (2008) Cognitive neuroscience of aging. Ann N Y Acad Sci 1124:127–144

Grady CL (2012) The cognitive neuroscience of ageing. Nat Rev Neurosci 13:491–505

Grady CL, Maisog JM, Horwitz B, Ungerleider LG, Mentis MJ, Salerno JA, Pietrini P, Wagner E, Haxby JV (1994) Age-related changes in cortical blood flow activation during visual processing of faces and location. J Neurosci 14(Pt 2):1450–1462

Grady CL, Springer MV, Hongwanishkul D, McIntosh AR, Winocur G (2006) Age- related changes in brain activity across the adult lifespan. J Cogn Neurosci 18:227–241

Grady CL, Sarraf S, Saverino C, Campbell K (2016) Age differences in the functional interactions among the default, frontoparietal control, and dorsal attention networks. Neurobiol Aging 41:159–172

Greve DN, Fischl B (2009) Accurate and robust brain image alignment using boundary- based registration. NeuroImage 48:63–72

Griffanti L, Salimi-Khorshidi G, Beckmann CF, Auerbach EJ, Douaud G, Sexton CE, Zsoldos E, Ebmeier KP, Filippini N, Mackay CE, Moeller S, Xu J, Yacoub E, Baselli G, Ugurbil K, Miller KL, Smith SM (2014) ICA-based artefact removal and accelerated fMRI acquisition for improved resting state network imaging. NeuroImage 95(C5):232–247

Griffanti L, Douaud G, Bijsterbosch J, Evangelisti S, Alfaro-Almagro F, Glasser MF, Fuff EP, Fitzgibbon S, Westphal R, Carone D, Beckmann CF, Smith SM (2017) Hand classification of fMRI ICA noise components. NeuroImage 154:188–205

Griswold MA, Jakob PM, Heidemann RM, Nittka M, Jellus V, Wang J, Kiefer B, Haase A (2002) Generalized autocalibrating partially parallel acquisitions (GRAPPA). Magn Reson Med 47:1202–1210

Gutchess AH, Welsh RC, Hedden T, Bangert A, Minear M, Liu LL, Park DC (2005) Aging and the neural correlates of successful picture encoding: frontal activations compensate for decreased medial-temporal activity. J Cogn Neurosci 17:84–96

Hachinski VC, Iliff LD, Zilhka E, Du Boulay GH, McAllister VL, Marshall J, Russel RW, Symon L (1975) Cerebral blood flow in dementia. Arch Neurol 32:632–637

Hampson M, Tokoglu F, Shen X, Scheinost D, Papademetris X, Constable RT (2012) Intrinsic brain connectivity related to age in young and middle aged adults. PLoS ONE 7:e44067

Han L, Savalia NK, Chan MY, Agres PF, Nair AS, Wig GS (2018) Functional parcellation of the cerebral cortex across the human adult lifespan. Cereb Cortex 28:4403–4423

Handwerker DA, Gazzaley A, Inglis BA, D'Esposito M (2007) Reducing vascular variability of fMRI data across aging populations using a breathholding task. Hum Brain Mapp 28:846–859

Hedden T, Gabrieli JDE (2004) Insights into the ageing mind: a view from cognitive neuroscience. Nat Rev Neurosci 5:87–96

Hesselmann V, Zaro Weber O, Wedekind C, Krings T, Schulte O, Kugel H, Krug B, Klug N, Lackner KJ (2001) Age related signal decrease in functional magnetic resonance imaging during motor stimulation in humans. Neurosci Lett 308:141–144

Hillman EMC (2014) Coupling mechanism and significance of the BOLD signal: a status report. Annu Rev Neurosci 37:161–181

Himberg J, Hyvärinen A, Esposito F (2004) Validating the independent components of neuroimaging time series via clustering and visualization. NeuroImage 22:1214–1222

Hirsiger S, Koppelmans V, Mérillat S, Liem F, Erdeniz B, Seidler RD, Jäncke L (2016) Structural and functional connectivity in healthy aging: associations for cognition and motor behavior. Hum Brain Mapp 37:855–867

Hochberg Y (1988) A sharper Bonferroni procedure for multiple tests of significance. Biometrika 75:800–802

Houx PJ, Jolles J (1993) Age-related decline of psychomotor speed: effects of age, brain health, sex, and education. Percept Mot Skills 76:195–211

Huang C-C, Hsieh W-J, Lee P-L, Peng L-N, Liu L-K, Lee W-J, Huang J-K, Chen L-K, Lin C-P (2015) Age-related changes in resting-state networks of a large sample size of healthy elderly. CNS Neurosci Ther 21:817–825

Hughes CP, Berg L, Danziger WL, Coben LA, Martin RL (1982) A new clinical scale for the staging of dementia. Br J Psychiatry 140:566–572

Hutchinson S, Kobayashi M, Horkan CM, Pascual-Leone A, Alexander MP, Schlaug G (2002) Age-related differences in movement representation. NeuroImage 17:1720–1728

Hutchison JL, Lu H, Rypma B (2013) Neural mechanisms of age-related slowing: the $\Delta CBF/\Delta CMRO_2$ ratio mediates age-differences in BOLD signal and human performance. Cereb Cortex 23:2337–2346

Jenkinson M, Bannister P, Brady M, Smith S (2002) Improved optimization for the robust and accurate linear registration and motion correction of brain images. NeuroImage 17:825–841

Kannurpatti SS, Motes MA, Rypma B, Biswal BB (2011) Increasing measurement accuracy of age-related BOLD signal change: minimizing vascular contributions by resting- state-fluctuation-of-amplitude scaling. Hum Brain Mapp 32:1125–1140

Kauranen K, Vanharanta H (1996) Influences of aging, gender, and handedness on motor performance of upper and lower extremities. Percept Mot Skills 82:515–525

Keller JB, Hedden T, Thompson TW, Anteraper SA, Gabrieli JDE, Whitfield- Gabrieli S (2015) Resting-state anticorrelations between medial and lateral prefrontal cortex: association with working memory, aging, and individual differences. Cortex 64:271–280

Kety SS (1956) Human cerebral blood flow and oxygen consumption as related to aging. J Chronic Dis 3:478–486

Kim S-G (2018) Biophysics of BOLD fMRI investigated with animal models. J Magn Reson 292:82–89

Kim SG, Ogawa S (2012) Biophysical and physiological origins of blood oxygenation level-dependent fMRI signals. J Cereb Blood Flow Metab 32:1188–1206

Kim J-H, Lee Y-S, Lee J-J, Song H-J, Yoo D-S, Lee HJ, Kim H-J, Chang Y (2010) Functional magnetic resonance imaging reveals age-related alterations to motor networks in weighted elbow flexion-extension movement. Neurol Res 32:995–1001

Koch W, Teipel S, Mueller S, Buerger K, Bokde ALW, Hampel H, Coates U, Reiser M, Meindl T (2010) Effects of aging on default mode network activity in resting state fMRI: does the method of analysis matter? NeuroImage 51:280–287

Laumann TO, Gordon EM, Adeyemo B, Snyder AZ, Joo SJ, Chen M-Y, Gilmore AW, McDermott KB, Nelson SM, Dosenbach NUF, Schlaggar BL, Mumford JA, Poldrack RA, Petersen SE (2015) Functional system and areal organization of a highly sampled individual human brain. Neuron 87:657–670

Lawrence KD, Shier DR (1981) A comparison of least squares and least absolute deviation regression models for estimating Weibull parameters. Commun Stat Simulation Computa 10:315–326

Leong RLF, Lo JC, Sim SKY, Zheng H, Tandi J, Zhou J, Chee MWL (2017) Longitudinal brain structure and cognitive changes over 8 years in an East Asian cohort. NeuroImage 147:852–860

Levine BK, Beason-Held LL, Purpura KP, Aronchick DM, Optican LM, Alexander GE, Horwitz B, Rapoport SI, Schapiro MB (2000) Age-related differences in visual perception: a PET study. Neurobiol Aging 21:577–584

Li H-J, Hou X-H, Liu H-H, Yue C-L, Lu G-M, Zuo X-N (2015) Putting age-related task activation into large-scale brain networks: a meta-analysis of 114 fMRI studies on healthy aging. Neurosci Biobehav Rev 57:156–174

Liao X, Cao M, Xia M, He Y (2017) Individual differences and time-varying features of modular brain architecture. NeuroImage 152:94–107

Liu P, Hebrank AC, Rodrigue KM, Kennedy KM, Section J, Park DC, Lu H (2013) Age-related differences in memory-encoding fMRI responses after accounting for decline in vascular reactivity. NeuroImage 78:415–425

Logan JM, Sanders AL, Snyder AZ, Morris JC, Buckner RL (2002) Under- recruitment and nonselective recruitment: dissociable neural mechanisms associated with aging. Neuron 33:827–840

Logothetis NK, Pauls J, Augath M, Trinath T, Oeltermann A (2001) Neurophysiological investigation of the basis of the fMRI signal. Nature 412:150–157

Lu H, Xu F, Rodrigue KM, Kennedy KM, Cheng Y, Flicker B, Hebrank AC, Uh J, Park DC (2011) Alterations in cerebral metabolic rate and blood supply across the adult lifespan. Cereb Cortex 21:1426–1434

Lustig C, Snyder AZ, Bhakta M, O'Brien KC, McAvoy M, Raichle ME, Morris JC, Buckner RL (2003) Functional deactivations: change with age and dementia of the Alzheimer type. Proc Natl Acad Sci 100:14504–14509

Madan CR (2018) Age differences in head motion and estimates of cortical morphology. PeerJ 6:e5176

Madden DJ, Turkington TG, Coleman RE, Provenzale JM, DeGrado TR, Hoffman JM (1996) Adult age differences in regional cerebral blood flow during visual world identification: evidence from $H_2{}^{15}O$ PET. NeuroImage 3:127–142

Malykhin NV, Huang Y, Hrybouski S, Olsen F (2017) Differential vulnerability of hippocampal subfields and anteroposterior hippocampal subregions in healthy cognitive aging. Neurobiol Aging 59:121–134

Mattay VS, Fera F, Tessitore A, Hariri AR, Das S, Callicott JH, Weinberger DR (2002) Neurophysiological correlates of age-related changes in human motor function. Neurology 58:630–635

McDonald CR, McEvoy LK, Gharapetian L, Fennema-Notestine C, Hagler DJ, Holland D, Koyama A, Brewer JB, Dale AM (2009) Regional rates of neocortical atrophy from normal aging to early Alzheimer disease. Neurology 73:457–465

Mehagnoul-Schipper DJ, van der Kallen BFW, Colier WNJM, van der Sluijs MC, van Erning LJTO, Thijssen HOM, Oeseburg B, Hoefnagels WHL, Jansen RWMM (2002) Simultaneous measurements of cerebral oxygenation changes during brain activation by near-infrared spectroscopy and functional magnetic resonance imaging in healthy young and elderly subjects. Hum Brain Mapp 16:14–23

Meier TB, Desphande AS, Vergun S, Nair VA, Song J, Biswal BB, Meyerand ME, Birn RM, Prabhakaran V (2012) Support vector machine classification and characterization of age-related reorganization of functional brain networks. NeuroImage 60:601–613

Melamed E, Lavy S, Bentin S, Cooper G, Rinot Y (1980) Reduction in regional cerebral blood flow during normal aging in man. Stroke 11:31–35

Meunier D, Achard S, Morcom A, Bullmore E (2009) Age-related changes in modular organization of human brain functional networks. NeuroImage 44:715–723

Miller SL, Celone K, DePeau K, Diamond E, Dickerson BC, Rentz D, Pihlajamäki M, Sperling RA (2008) Age-related memory impairment associated with loss of parietal deactivation but preserved hippocampal activation. Proc Natl Acad Sci USA 105:2181–2186

Mitra P, Bokil H (2008) Observed brain dynamics. Oxford University Press, New York

Morrison JH, Baxter MG (2012) The ageing cortical synapse: hallmarks and implications for cognitive decline. Nat Rev Neurosci 13:240–250

Mowinckel AM, Espeseth T, Westlye LT (2012) Network-specific effects of age and in- scanner subject motion: a resting-state fMRI study of 238 healthy adults. NeuroImage 63:1364–1373

Mueller S, Wang D, Fox MD, Yeo BTT, Sepulcre J, Sabuncu MR, Shafee R, Lu J, Liu H (2013) Individual variability in functional connectivity architecture of the human brain. Neuron 77:586–595

Nasreddine ZS, Phillips NA, Bédirian V, Charbonneau S, Whitehead V, Collin I, Cummings JL, Chertkow H (2005) The Montreal cognitive assessment, MoCA: a brief screening tool for mild cognitive impairment. J Am Geriatr Soc 53:695–699

Nelder JA, Mead R (1965) A simplex method for function minimization. Comput J 7:308–313

Ng KK, Lo JC, Lim JKW, Chee MWL, Zhou J (2016) Reduced functional segregation between the default mode network and the executive control network in healthy older adults: a longitudinal study. NeuroImage 133:321–330

Oldfield RC (1971) The assessment and analysis of handedness: the Edinburgh inventory. Neuropsychologia 9:97–113

Onoda K, Yamaguchi S (2013) Small-worldness and modularity of the resting-state functional brain network decrease with aging. Neurosci Lett 556:104–108

Onoda K, Ishihara M, Yamaguchi S (2012) Decreased functional connectivity by aging is associated with cognitive decline. J Cogn Neurosci 24:2186–2198

Park DC, Reuter-Lorenz P (2009) The adaptive brain: aging and neurocognitive scaffolding. Annu Rev Psychol 60:173–196

Park DC, Welsh RC, Marshuetz C, Gutchess AH, Mikels J, Polk TA, Noll DC, Taylor SF (2003) Working memory for complex scenes: age differences in frontal and hippocampal activations. J Cogn Neurosci 15:1122–1134

Park DC, Polk TA, Park R, Minear M, Savage A, Smith MR (2004) Aging reduces neural specialization in ventral visual cortex. Proc Natl Acad Sci 101:13091–13095

Park DC, Polk TA, Hebrank AC, Jenkins LJ (2010) Age differences in default mode activity on easy and difficult spatial judgment tasks. Front Human Neurosci 3:7

Peng S-L, Dumas JA, Park DC, Liu P, Filbey FM, McAdams CJ, Pinkham AE, Adinoff B, Zhang R, Lu H (2014) Age-related increase of resting metabolic rate in the human brain. NeuroImage 98:176–183

Persson J, Lustig C, Nelson JK, Reuter-Lorenz PA (2007) Age differences in deactivation - a link to cognitive control? J Cogn Neurosci 19:1021–1032

Persson J, Pudas S, Nilsson L-G, Nyberg L (2014) Longitudinal assessment of default- mode brain function in aging. Neurobiol Aging 35:2107–2117

Petersen SE, Posner MI (2012) The attention system of the human brain: 20 years after. Neuroscience 35:73–89

Power JD, Cohen AL, Nelson SM, Wig GS, Barnes KA, Church JA, Vogel AC, Laumann TO, Miezin FM, Schlaggar BL, Petersen SE (2011) Functional network organization of the human brain. Neuron 72:665–678

Power JD, Barnes KA, Snyder AZ, Schlaggar BL, Petersen SE (2012) Spurious but systematic correlations in functional connectivity MRI networks arise from subject motion. NeuroImage 59:2142–2154

Power JD, Silver BM, Silverman MR, Ajodan EL, Bos DJ, Jones RM (2019) Customized head molds reduce motion during resting state fMRI scans. NeuroImage 189:141–149

Pruim RHR, Mennes M, van Rooij D, Llera A, Buitelaar JK, Beckmann CF (2015a) ICA-AROMA: A robust ICA-based strategy for removing motion artifacts from fMRI data. NeuroImage 112:267–277

Pruim RHR, Mennes M, Buitelaar JK, Beckmann CF (2015b) Evaluation of ICA- AROMA and alternative strategies for motion artifact removal in resting state fMRI. NeuroImage 112:278–287

Raichle ME, Snyder AZ (2007) A default mode of brain function: a brief history of an evolving idea. NeuroImage 37:1083–1090

Rajah MN, D'Esposito M (2005) Region-specific changes in prefrontal function with age: a review of PET and fMRI studies on working and episodic memory. Brain 128(Pt 9):1964–1983

Raz N, Gunning FM, Head D, Dupuis JH, McQuain J, Briggs SD, Loken WJ, Thornton AE, Acker JD (1997) Selective aging of the human cerebral cortex observed in vivo: differential vulnerability of the prefrontal gray matter. Cereb Cortex 7:268–282

Raz N, Gunning-Dixon F, Head D, Rodrigue KM, Williamson A, Acker JD (2004) Aging, sexual dimorphism, and hemispheric asymmetry of the cerebral cortex: replicability of regional differences in volume. Neurobiol Aging 25:377–396

Raz N, Lindenberger U, Rodrigue KM, Kennedy KM, Head D, Williamson A, Dahle C, Gerstorf D, Acker JD (2005) Regional brain changes in aging healthy adults: general

trends, individual differences and modifiers. Cereb Cortex 15:1676–1689
Raz N, Ghisletta P, Rodrigue KM, Kennedy KM, Lindenberger U (2010) Trajectories of brain aging in middle-aged and older adults: regional and individual differences. NeuroImage 51:501–511
Resnick SM, Pham DL, Kraut MA, Zonderman AB, Davatzikos C (2003) Longitudinal magnetic resonance imaging studies of older adults: a shrinking brain. J Neurosci 23:3295–3301
Reuter-Lorenz PA, Cappell KA (2008) Neurocognitive aging and the compensation hypothesis. Current Directions Psychol Sci 17:177–182
Rieck JR, Rodrigue KM, Kennedy KM, Devous MD, Park DC (2015) The effect of beta-amyloid on face processing in young and old adults: a multivariate analysis of the BOLD signal. Hum Brain Mapp 36:2514–2526
Riecker A, Gröschel K, Ackermann H, Steinbrink C, Witte O, Kastrup A (2006) Functional significance of age-related differences in motor activation patterns. NeuroImage 32:1345–1354
Robinson S, Basso G, Soldati N, Sailer U, Jovicich J, Bruzzone L, Kryspin-Exner I, Bauer H, Moser E (2009) A resting state network in the motor control circuit of the basal ganglia. BMC Neurosci 10:137
Ross MH, Yurgelun-Todd DA, Renshaw PF, Maas LC, Mendelson JH, Mello NK, Cohen BM, Levin JM (1997) Age-related reduction in functional MRI response to photic stimulation. Neurology 48:173–176
Rossi S, Miniussi C, Pasqualetti P, Babiloni C, Rossini PM, Cappa SF (2004) Age- related functional changes of prefrontal cortex in long-term memory: a repetitive transcranial magnetic stimulation study. J Neurosci 24:7939–7944
Royston P, Altman DG (1994) Regression using fractional polynomials of continuous covariates: parsimonious parametric modelling. Appl Stat 43:429
Rubinov M, Sporns O (2010) Complex network measures of brain connectivity: uses and interpretations. NeuroImage 52:1059–1069
Rypma B, D'Esposito M (2000) Isolating the neural mechanisms of age-related changes in human working memory. Nat Neurosci 3:509–515
Sala-Llonch R, Bartrés-Faz D, Junqué C (2015) Reorganization of brain networks in aging: a review of functional connectivity studies. Front Psychol 6:663
Salimi-Khorshidi G, Douaud G, Beckmann CF, Glasser MF, Griffanti L, Smith SM (2014) Automatic denoising of functional MRI data: combining independent component analysis and hierarchical fusion of classifiers. NeuroImage 90:449–468
Sambataro F, Murty VP, Callicott JH, Tan H-Y, Das S, Weinberger DR, Mattay VS (2010) Age-related alterations in default mode network: impact on working memory performance. Neurobiol Aging 31:839–852
Sauerbrei W, Royston P (1999) Building multivariable prognostic and diagnostic models: transformation of the predictors by using fractional polynomials. J Royal Stat Soc Series A (Statistics in Society) 162:71–94
Sauerbrei W, Meier-Hirmer C, Benner A, Royston P (2006) Multivariable regression model building by using fractional polynomials: Description of SAS, STATA and R programs. Comput Stat Data Anal 50:3464–3485
Schneider-Garces NJ, Gordon BA, Brumback-Peltz CR, Shin E, Lee Y, Sutton BP, Maclin EL, Gratton G, Fabiani M (2010) Span, CRUNCH, and beyond: working memory capacity and the aging brain. J Cogn Neurosci 22:655–669
Schroeder W, Martin K, Lorensen B (2006) Visualization Toolkit: An Object-Oriented Approach to 3D Graphics, 4th Edition. Kitware, ISBN 978-1-930934-19-1
Sled JG, Zijdenbos AP, Evans AC (1998) A nonparametric method for automatic correction of intensity nonuniformity in MRI data. IEEE Trans Med Imaging 17:87–97
Smith SM, Nichols TE (2009) Threshold-free cluster enhancement: addressing problems of smoothing, threshold dependence and localisation in cluster inference. NeuroImage 44:83–98
Smith SM, Jenkinson M, Woolrich MW, Beckmann CF, Behrens TEJ, Johansen- Berg H, Bannister PR, De Luca M, Drobnjak I, Flitney DE, Niazy RK, Saunders J, Vickers J, Zhang Y, De Stefano N, Brady JM, Matthews PM (2004) Advances in functional and structural MR image analysis and implementation as FSL. NeuroImage 23(Suppl 1):S208–S219
Smith SM, Fox PT, Miller KL, Glahn DC, Fox PM, Mackay CE, Filippini N, Watkins KE, Toro R, Laird AR, Beckmann CF (2009) Correspondence of the brain's functional architecture during activation and rest. Proc Natl Acad Sci USA 106:13040–13045
Smith SM, Miller KL, Salimi-Khorshidi G, Webster M, Beckmann CF, Nichols TE, Ramsey JD, Woolrich MW (2011) Network modelling methods for FMRI. NeuroImage 54(2):875–891
Solé-Padullés C, Bartrés-Faz D, Junqué C, Clemente IC, Molinuevo JL, Bargalló N, Sánchez-Aldeguer J, Bosch B, Falcón C, Valls-Solé J (2006) Repetitive transcranial magnetic stimulation effects on brain function and cognition among elders with memory dysfunction. A randomized sham-controlled study. Cereb Cortex 16:1487–1493
Song J, Birn RM, Boly M, Meier TB, Nair VA, Meyerand ME, Prabhakaran V (2014) Age-related reorganizational changes in modularity and functional connectivity of human brain networks. Brain Connectivity 4:662–676
Sperling R (2007) Functional MRI studies of associative encoding in normal aging, mild cognitive impairment, and Alzheimer's disease. Ann N Y Acad Sci 1097:146–155
Spreng RN, Wojtowicz M, Grady CL (2010) Reliable differences in brain activity between young and old adults: a quantitative meta-analysis across multiple cognitive domains. Neurosci Biobehav Rev 34:1178–1194
Spreng RN, Stevens WD, Viviano JD, Schacter DL (2016) Attenuated anticorrelation between the default and dorsal attention networks with aging: evidence from task and rest. Neurobiol Aging 45:149–160
Stefanova I, Stephan T, Becker-Bense S, Dera T, Brandt T, Dieterich M (2013) Age- related changes of blood-oxygen-level-dependent signal dynamics during optokinetic stimulation. Neurobiol Aging 34:2277–2286
Sugiura M (2016) Functional neuroimaging of normal aging: declining brain, adapting brain. Ageing Res Rev 30:61–72
Tao H, Guo S, Ge T, Kendrick KM, Xue Z, Liu Z, Feng J (2013) Depression uncouples brain hate circuit. Mol Psychiatry 18:101–111
Taoka T, Iwasaki S, Uchida H, Fukusumi A, Nakagawa H, Kichikawa K, Takayama K, Yoshioka T, Takewa M, Ohishi H (1998) Age correlation of the time lag in signal change on EPI-fMRI. J Comput Assist Tomogr 22:514–517
Tomasi D, Volkow ND (2012) Aging and functional brain networks. Mol Psychiatry 17(5):549–558
Tsvetanov KA, Henson RNA, Tyler LK, Davis SW, Shafto MA, Taylor JR, Williams N, Cam-CAN, Rowe JB (2015) The effect of ageing on fMRI: correction for the confounding effects of vascular reactivity evaluated by joint fMRI and MEG in 335 adults. Hum Brain Mapp 36:2248–2269
Uludağ K, Blinder P (2018) Linking brain vascular physiology to hemodynamic response in ultra-high field MRI. NeuroImage 168:279–295
Uludağ K, Müller-Bierl B, Ugurbil K (2009) An integrative model for neuronal activity- induced signal changes for gradient and spin echo functional imaging. NeuroImage 48:150–165

van Wijk BCM, Stam CJ, Daffertshofer A (2010) Comparing brain networks of different size and connectivity density using graph theory. PLoS ONE 5(10):e13701

van Dijk KRA, Sabuncu MR, Buckner RL (2012) The influence of head motion on intrinsic functional connectivity MRI. NeuroImage 59:431–438

van den Heuvel MP, de Lange SC, Zalesky A, Seguin C, Yeo BTT, Schmidt R (2017) Proportional thresholding in resting-state fMRI functional connectivity networks and consequences for patient-control connectome studies: issues and recommendations. NeuroImage 152:437–449

Vij SG, Nomi JS, Dajani DR, Uddin LQ (2018) Evolution of spatial and temporal features of functional brain networks across the lifespan. NeuroImage 173:498–508

Wang L, Li Y, Metzak P, He Y, Woodward TS (2010) Age-related changes in topological patterns of large-scale brain functional networks during memory encoding and recognition. NeuroImage 50:862–872

Wang M, Gamo NJ, Yang Y, Jin LE, Wang X-J, Laubach M, Mazer JA, Lee D, Arnsten AFT (2011) Neuronal basis of age-related working memory decline. Nature 476:210–213

Ward LM, Aitchison RT, Tawse M, Simmers AJ, Shahani U (2015) Reduced haemodynamic response in the ageing visual cortex measured by absolute fNIRS. PLoS ONE 10:e0125012

West KL, Zuppichini MD, Turner MP, Sivakolundu DK, Zhao Y, Abdelkarim D, Spence JS, Rypma B (2019) BOLD hemodynamic response function changes significantly with healthy aging. NeuroImage 188:198–207

Wig GS (2017) Segregated Systems of Human Brain Networks. Trends Cogn Sci 21:981–996

Wig GS, Laumann TO, Petersen SE (2014) An approach for parcellating human cortical areas using resting-state correlations. NeuroImage 93(Pt 2):276–291

Wimble M, Yoder M, Ro YK (2016) Understanding least absolute value in regression- based data mining. Int J Data Mining Knowledge Manage Process 6:1–10

Wright ME, Wise RG (2018) Can blood oxygenation level dependent functional magnetic resonance imaging be used accurately to compare older and younger populations? A mini literature review. Front Aging Neurosci 10:371

Wu J-T, Wu H-Z, Yan C-G, Chen W-X, Zhang H-Y, He Y, Yang H-S (2011) Aging-related changes in the default mode network and its anti-correlated networks: a resting- state fMRI study. Neurosci Lett 504:62–67

Yamaguchi T, Kanno I, Uemura K, Shishido F, Inugami A, Ogawa T et al (1986) Reduction in regional cerebral metabolic rate of oxygen during human aging. Stroke 17(6):1220–1228

Yan L, Zhuo Y, Wang B, Wang DJJ (2011) Loss of coherence of low frequency fluctuations of BOLD FMRI in visual cortex of healthy aged subjects. Open Neuroimaging J 5(Suppl 1):105–111

Yeo BTT, Krienen FM, Sepulcre J, Sabuncu MR, Lashkari D, Hollinshead M, Roffman JL, Smoller JW, Zöllei L, Polimeni JR, Fischl B, Liu H, Buckner RL (2011) The organization of the human cerebral cortex estimated by intrinsic functional connectivity. J Neurophysiol 106:1125–1165

Yeo BTT, Krienen FM, Chee MWL, Buckner RL (2014) Estimates of segregation and overlap of functional connectivity networks in the human cerebral cortex. NeuroImage 88:212–227

Yesavage JA, Brink TL, Rose TL, Lum O, Huang V, Adey M, Leirer VO (1982) Development and validation of a geriatric depression screening scale: a preliminary report. J Psychiatr Res 17:37–49

Zalesky A, Fornito A, Bullmore E (2012) On the use of correlation as a measure of network connectivity. NeuroImage 60:2096–2106

Zhang N, Gordon ML, Goldberg TE (2017) Cerebral blood flow measured by arterial spin labeling MRI at resting state in normal aging and Alzheimer's disease. Neurosci Biobehav Rev 72:168–175

Zhu Y, Cribben I (2018) Sparse graphical models for functional connectivity networks: best methods and the autocorrelation issue. Brain Connectivity 8:139–165

Zonneveld HI, Pruim RH, Bos D, Vrooman HA, Muetzel RL, Hofman A, Rombouts SARB, van der Lugt A, Niessen WJ, Ikram MA, Vernooij MW (2019) Patterns of functional connectivity in an aging population: the Rotterdam Study. NeuroImage 189:432–444